LARGE-SCALE TEMPERATURE CHANGES ACROSS THE SOUTHERN ANDES: 20TH-CENTURY VARIATIONS IN THE CONTEXT OF THE PAST 400 YEARS

RICARDO VILLALBA [1], ANTONIO LARA [2], JOSÉ A. BONINSEGNA [1], MARIANO MASIOKAS [1], SILVIA DELGADO [1], JUAN C. ARAVENA [3], FIDEL A. ROIG [1], ANDREA SCHMELTER [4], ALEXIA WOLODARSKY [2] and ALBERTO RIPALTA [1]

[1] *Departamento de Dendrocronología e Historia Ambiental, Instituto Argentino de Nivología, Glaciología y Ciencias Ambientales (IANIGLA), C.C. 330, 5500 Mendoza, Argentina*
E-mail: ricardo@lab.cricyt.edu.ar
[2] *Instituto de Silvicultura, Universidad Austral de Chile, Casilla 567, Valdivia, Chile*
[3] *Laboratorio de Botánica, Universidad de Chile, Casilla 3576, Santiago, Chile*
[4] *Geographisch Institut der Universität Bonn, Meckenheimer 166, 53115 Bonn, Germany*

Abstract. Long-term trends of temperature variations across the southern Andes (37–55° S) are examined using a combination of instrumental and tree-ring records. A critical appraisal of surface air temperature from station records is presented for southern South America during the 20th century. For the interval 1930–1990, three major patterns in temperature trends are identified. Stations along the Pacific coast between 37 and 43° S are characterized by negative trends in mean annual temperature with a marked cooling period from 1950 to the mid-1970s. A clear warming trend is observed in the southern stations (south of 46° S), which intensifies at higher latitudes. No temperature trends are detected for the stations on the Atlantic coast north of 45° S. In contrast to higher latitudes in the Northern Hemisphere where annual changes in temperature are dominated by winter trends, both positive and negative trends in southern South America are due to mostly changes in summer (December to February) temperatures. Changes in the Pacific Decadal Oscillation (PDO) around 1976 are felt in summer temperatures at most stations in the Pacific domain, starting a period with increased temperature across the southern Andes and at higher latitudes. Tree-ring records from upper-treeline were used to reconstruct past temperature fluctuations for the two dominant patterns over the southern Andes. These reconstructions extend back to 1640 and are based on composite tree-ring chronologies that were processed to retain as much low-frequency variance as possible. The resulting reconstructions for the northern and southern sectors of the southern Andes explain 55% and 45% of the temperature variance over the interval 1930–1989, respectively. Cross-spectral analysis of actual and reconstructed temperatures over the common interval 1930–1989, indicates that most of the explained variance is at periods >10 years in length. At periods >15 years, the squared coherency between actual and reconstructed temperatures ranges between 0.6 and 0.95 for both reconstructions. Consequently, these reconstructions are especially useful for studying multi-decennial temperature variations in the South American sector of the Southern Hemisphere over the past 360 years. As a result, it is possible to show that the temperatures during the 20th century have been anomalously warm across the southern Andes. The mean annual temperatures for the northern and southern sectors during the interval 1900–1990 are 0.53 °C and 0.86 °C above the 1640–1899 means, respectively. These findings placed the current warming in a longer historical perspective, and add new support for the existence of unprecedented 20th century warming over much of the globe. The rate of temperature increase from 1850 to 1920 was the highest over the past 360 years, a common feature observed in several proxy records from higher latitudes in the Northern Hemisphere.

Local temperature regimes are affected by changes in planetary circulation, with in turn are linked to global sea surface temperature (SST) anomalies. Therefore, we explored how temperature variations in the southern Andes since 1856 are related to large-scale SSTs on the South Pacific and South Atlantic Oceans. Spatial correlation patterns between the reconstructions and SSTs show that temperature variations in the northern sector of the southern Andes are strongly connected with SST anomalies in the tropical and subtropical Pacific. This spatial correlation pattern resembles the spatial signature of the PDO mode of SST variability over the South Pacific and is connected with the Pacific-South American (PSA) atmospheric pattern in the Southern Hemisphere. In contrast, temperature variations in the southern sector of the southern Andes are significantly correlated with SST anomalies over most of the South Atlantic, and in less degree, over the subtropical Pacific. This spatial correlation field regressed against SST resembles the 'Global Warming' mode of SST variability, which in turn, is linked to the leading mode of circulation in the Southern Hemisphere. Certainly, part of the temperature signal present in the reconstructions can be expressed as a linear combination of four orthogonal modes of SST variability. Rotated empirical orthogonal function analysis, performed on SST across the South Pacific and South Atlantic Oceans, indicate that four discrete modes of SST variability explain a third, approximately, of total variance in temperature fluctuations across the southern Andes.

1. Introduction

Several authors have analyzed the instrumental record of mean surface temperatures from the Southern Hemisphere with fairly similar results (WMO, 1998). The mean hemispheric temperature has increased by about 0.3 to 0.6 °C since the late 19th century, and by about 0.2 to 0.3 °C since mid-1970s. The trend was almost zero prior to 1910. The warming occurred largely during two periods, between 1910 and 1940 and since the mid-1970s. However, there are large areas in the Southern Hemisphere devoid of long and consistent temperature records where temperature trends remain undocumented. Among the least known areas in the Southern Hemisphere are the higher latitudes in South America where very little information is available.

It is extremely difficult to document the long-term temperature changes during the 20th century at the southern latitudes (40–60° S) due to the poor quality of the instrumental data and the small number of meteorological stations. Time series are short, fragmentary, and suffer from serious drawbacks due to undocumented changes in instrumentation and station locations (Rosemblüt et al., 1997). In addition, the instrumental data provide only a limited temporal perspective on present climate. How unusual was the climate in southern South America during the last century when it is placed in the longer-term context of climate variations for the past centuries? To overcome some of these limitations, we combined station and tree-ring records from southern South America to provide the most consistent view of temperature variations during the 20th century and place these recent changes in the perspective of the past several centuries.

High-resolution paleoenvironmental records are essential to establish baselines for judging the anomalies of climatic changes in the 20th century, to evaluate

the response of ecosystems to natural climate variability, and to provide data for model verification (Bradley, 1999). The mountain environments in southern South America are excellent sources of paleoenvironmental records. Their physical and biological systems are highly sensitive to climatic variations and provide complementary records (e.g., tree-rings and glaciers) across a range of spatial and temporal resolutions (Villalba, 2000). The southern Andes spreads over a wide latitudinal range (37° to 55° S); along the west slope of southern South America, it encompasses a wide variety of climate regimes from the Mediterranean type with a dry summer in the north to a year-round rainy climate in the south (Figure 1). In addition, due to the proximity of the austral portion of the southern Andes to Antarctica, they represent the natural link between middle and high latitudes in the Southern Hemisphere.

Tree-ring records from high elevation sites provide climatically sensitive records that may extend over several centuries or more with annual to seasonal resolution. Recent efforts to increase our understanding of long-term climate variability across the Americas (Luckman and Boninsegna, 2001), have substantially increased the number of upper elevation chronologies in the southern Andes. More than 90 records from *Nothofagus pumilio*, the dominant subalpine species, have been developed in the southern Andes during the past 5 years. Techniques of temperature reconstructions have also undergone several developmental improvements since the initial attempts in the late 1980s (Boninsegna et al., 1989; Villalba et al., 1989; Villalba, 1990; Lara and Villalba, 1993). The increased number of high-elevation chronologies recently developed, the extension of the temporal coverage of these records, and the use of more conservative methods for standardization, now offer the opportunity of evaluating the past climate variations across the southern Andes (37–55° S) more consistently. By studying these records of past climate variability it should be possible to determine how unusual temperatures during the 20th century in the southern Andes has been in the context of the past centuries. Composite tree-ring chronologies from *Nothofagus pumilio* are used to reconstruct mean annual temperatures for the northern and southern sectors of the southern Andes from 1640 to the present.

SST anomalies are linked to changes in large-scale atmospheric circulation in the Southern Hemisphere and affect the temperature regimes across the southern Andes. Therefore, relationships between long-term changes in temperature recorded in the southern Andes and sea surface temperatures (SSTs) over the South Pacific and Atlantic Oceans were also examined.

2. Climate of the Southern Andes

There are no attempts to describe the climate of the southern Andes as a geographical unity. Most climate reviews deal independently with the Argentinean (De Fina, 1972; Prohaska, 1976) or the Chilean (Miller, 1976) sector of the southern
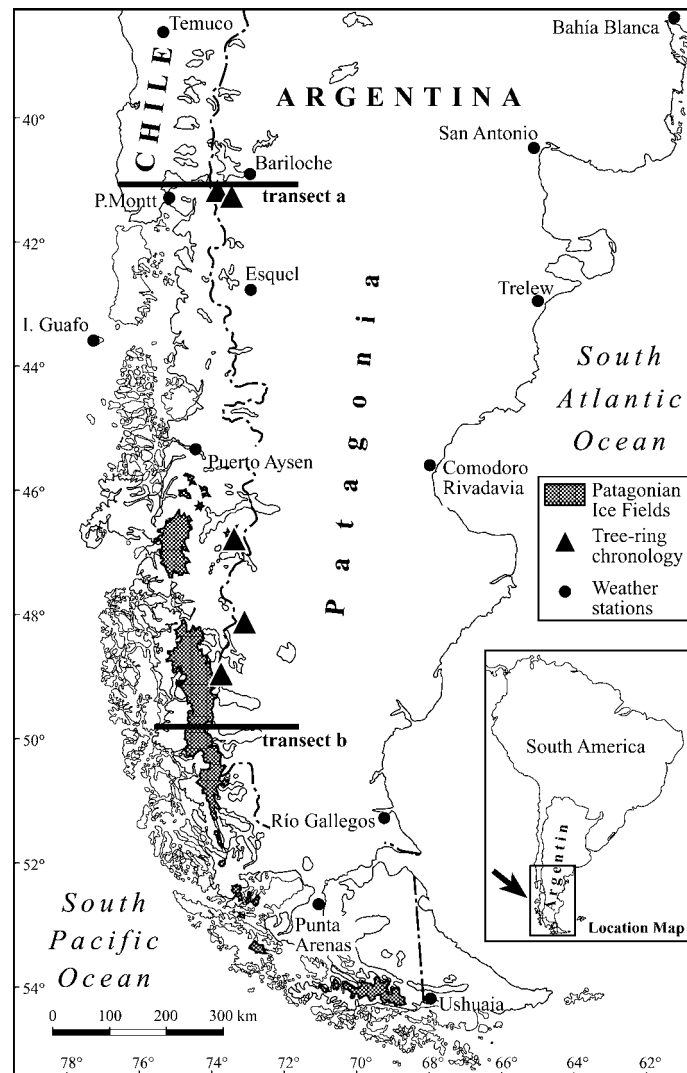
Figure 1. Map showing locations of meteorological stations (circles) and tree-ring records (triangles) used in this study. Geographical locations for the northern (transect a) and southern (transect b) transects across the southern Andes (shown in Figures 2 and 3) are also indicated.

Andes. Integration of data and information among these reviews is not always straightforward due to differences in the spatial scales considered (synoptic versus local). A major limitation for characterizing the climate of the southern Andes is the lack of meteorological records across large areas. Most records are not homogeneous and have large percentage of missing data. In addition, specificities of local microclimates within mountain environments exacerbate the problem of describing the regional climate on the basis of few meteorological records. Feedback mechanisms between the surface and the atmosphere, particularly vegetation

cover and geomorphological features create important microclimatic contrasts in surface heating, soil moisture or snow-cover duration (Geiger, 1965). The climate models overlook numerous climatological details of mountains, making it difficult to predict consequences of climate change on mountain hydrology, glaciers, or ecosystems (Beniston, 1994).

Climatically, the southern Andes (37–55° S) are located within the belt of the Southern Hemisphere westerlies with strong winds throughout the year (Figure 1). South of 40° S strong westerlies are remarkably persistent all year. The name given to latitudes south of 42° S is the 'roaring forties'. According to Schwerdtfeger (1960, 1962), this name could be extended well into the 'fifties'. At these latitudes, the direction of the wind is also remarkably persistent in the coastal region. A westerly component occurs at least 75% of the time along the entire coast (Miller, 1976). The annual frequency distribution of wind directions for individual stations on the eastern Patagonian plains show that westerly winds account for 50–70% of all observations. In the area next to the Andes, there is well-defined annual variation in wind direction due to small seasonal shifts of the predominant pressure systems (Prohaska, 1976).

Temperature patterns are highly influenced by latitude and elevation. For instance, mean annual temperature in the intermountain valleys of the southern Andes decreases from 12 °C in the north (37–42° S) to 6 °C toward the south (south of 47° S, Figures 2 and 3, respectively). Across Patagonia, mean temperature for the coldest (July) month ranges between 0 and 4 °C whereas for the warmest month (January) it ranges between 10 and 16 °C. Absolute minimum temperatures may be lower than –25 °C (Miller, 1976; Prohaska, 1976).

Across the west-east elevation gradient at 41° S, mean annual temperatures vary from 10 °C on the west side of the Andes, to 6 °C in the subalpine deciduous forest near treeline, and 8 °C at the steppe-forest transition east of the Andes (Almeyda and Saez, 1958; Gallopín, 1978). Annual thermal amplitudes across this gradient depend on the altitude, aspect, and proximity to the ocean being more marked on the Patagonian plains than on the Chilean side of the Andes (Figures 2 and 3). For west-exposed sites in the Andes such as Puerto Blest (41° S), the average diurnal temperature range is 6 °C. In closed valley within the cordillera or at the plains in the Patagonian plateau, the average diurnal temperature range may reach 10 °C or more.

The steady increase in both frequency and intensity of the westerlies with increasing latitude is reflected in more abundant rainfall toward the South and a reduced summer season (Miller, 1976; Prohaska, 1976; Figures 2 and 3). At Concepción, located at 36°40′ S, less than 6% of the total annual precipitation is recorded during summer (December to February), whereas at southern-located stations such as Valdivia (39°48′ S), Puerto Montt (41°28′ S) an San Pedro (47°43′ S), summer precipitation account for 9.7, 17.9, and 25.4% of the total annual, respectively. At San Pedro, precipitation is uniformly distributed over the year with no really dry months. The increase in precipitation during summer is largely respon-
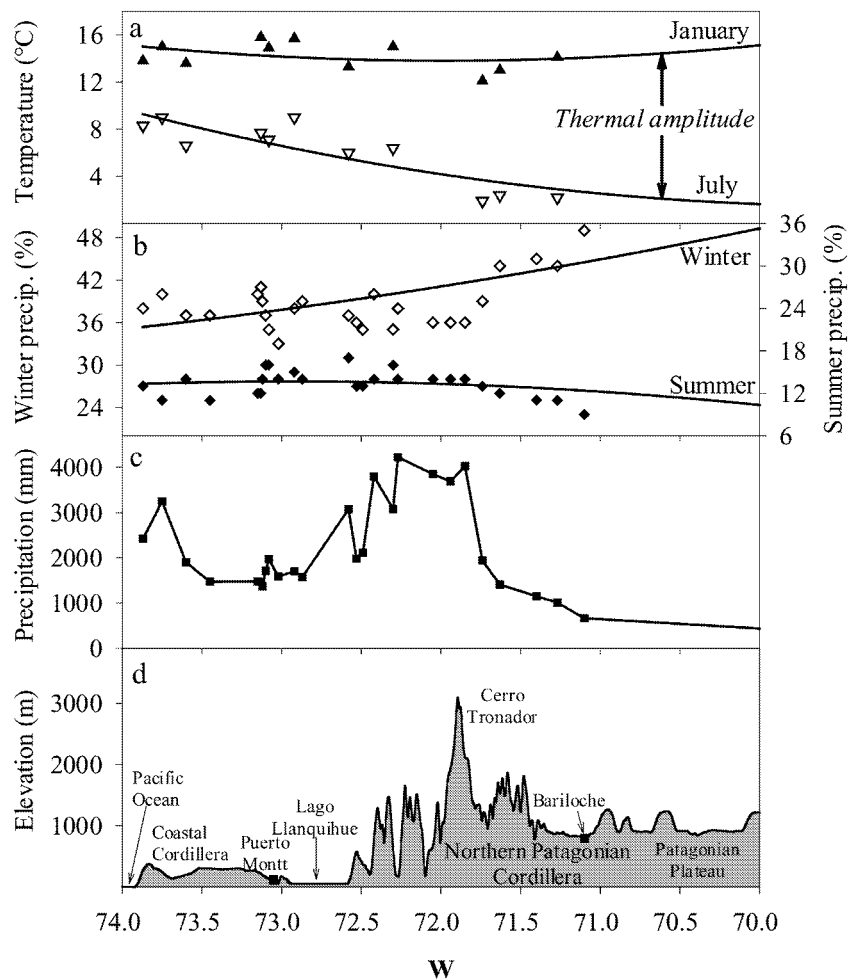
Figure 2. Transect across the southern Andes at approximately 41° S, showing changes in mean January and July temperatures (a), in seasonal (summer and winter) precipitation distribution (b), and in total annual precipitation (c) associated with topography (d) and distance from the Pacific Ocean. Locations of the meteorological stations are indicated by triangles (△) in (a), diamonds (◇) in (b), and squares (□) in (c). Meteorological stations in the latitudinal band between 40°30′ S and 41°30′ S have been included in this transect.

sible for the increased annual rainfall at the southern stations. For instance, the winter precipitation at Concepción is almost equal to that at Puerto Montt, but the latter receives almost 700 mm more than Concepcion during the rest of the year (Miller, 1976).

The interactions of the humid air masses from the Pacific with the mountain ranges determine a strong west-east gradient of precipitation across the region (Figures 2 and 3). In the northern sector of the southern Andes, orography accounts for the two maxima in precipitation at the Cordillera de la Costa (Coastal Range)
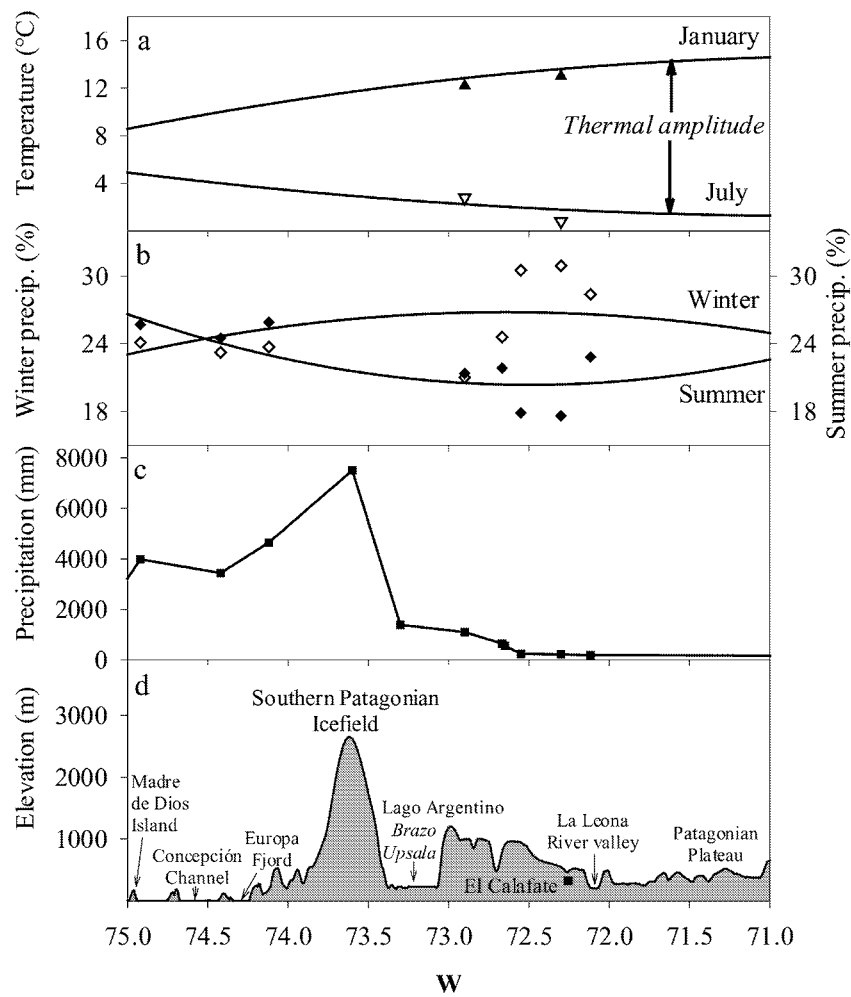
Figure 3. Transect across the southern Andes at approximately 51° S. Meteorological data are from stations located in the latitudinal band between 49° S and 53° S. For detailed key see Figure 2.

and the Cordillera de los Andes (main Cordillera). However, the effectiveness of the coastal range as a barrier to the westerly flow is reduced in comparison to the main Cordillera (Miller, 1976). Precipitation over the Andes increases with elevation, reaching a maximum close to the Andean crest. Precipitation is usually of the order of three to four times the amount over the low, western side at the same latitude. In winter, precipitation normally occurs as snow above 1000 m and 600 m in the northern and southern sectors of the southern Andes, respectively. Upper elevation valleys and mountain passes become inaccessible during winter due to heavy snow along the western slope of the Cordillera.

Precipitation decreases abruptly eastwards from the Andean crest. The west-to-east decrease on the lee side of the Andes is much greater than the increase on

its western side (Figures 2 and 3). At some points, precipitation decreases by a factor of twenty times in a distance of less than 100 km east of the ridgeline. At intermountain valleys such as the upper Río Manso valley (41° S), precipitation decreases 68% per 1000-m decrease in elevation and 5.2% per 1000 m in a west-east direction from the main ridgeline (Gallopín, 1978). In the foothills and the steppe, distance from the Andes explains more than 90% of the spatial variability of the mean annual precipitation (Jobbágy et al., 1995).

3. Instrumental Temperature Records

The complicating factors of local microclimates and great distances between stations often result in poor intercorrelations between station temperature records. We assembled all the available records from stations located between 36° and 55° S in Argentina and Chile. From a total of 31 temperature records, only 13 were selected due to the quality and extent of the records (interval 1930–1989, see Table I). Chilean records were obtained from the national Weather Service (Dirección Meteorológica de Chile), and most of the Argentinean records were extracted from The Global Historical Climatology Network (Vose et al., 1992). Many geographical gaps are evident in the distribution, most significantly between 46–51° S and across mainland Patagonia (Figure 1). A few stations do occur in these regions but the records are too short or fragmented for use in this study.

   Inhomogeneities in the Chilean records have been corrected by Rosenblüth et al. (1997). They used regression with the closest records to fill missing values. Homogeneity between series was accomplished by applying the test of Alexandersson (1986) to temperature differences between stations. Most of the Argentinean stations had complete records and few isolated months were filled following the same procedures used by Rosenblüth et al. (1997).

3.1. TEMPERATURE TRENDS

We selected two pair of records, the first at the northern (41° S) and the second at the southern (51° S) latitudes, to illustrate the temperature trends during the 20th century along the meridional gradient of the southern Andes. Puerto Montt and Bariloche represent temperate Mediterranean climates with winter maximum precipitation (Figure 2), whereas Punta Arenas and Río Gallegos correspond to cold climates with rainfall well distributed throughout the year (Figure 3). In both cases, the stations on the western side (Puerto Montt and Punta Arenas) are much moister than the stations on the lee side of the Andes (Bariloche) or on the Atlantic coast (Río Gallegos). Seasonal and annual temperature deviations from the interval 1960–1989 are shown in Figures 4 and 5. Smoothed versions of the temperature variations were obtaining by applying a cubic spline filter designed to maintain 50% of the variance at waves shorter than 15 years (Cook and Peters, 1981). Lineal

Table I

Meteorological stations: locations and records

Station	Latitude (°S)	Longitude (°W)	Data period	Source
Bahía Blanca	38°42′	62°12′	1920–1993	ORNL
Temuco	38°45′	72°38′	1930–1992	D. M. Chile
San Antonio Oeste	40°44′	64°57′	1930–1990	ORNL
Bariloche	41°12′	71°12′	1930–1996	ORNL
Puerto Montt	41°25′	73°05′	1930–1992	D. M. Chile
Esquel	42°45′	71°12′	1930–1996	ORNL
Trelew	43°13′	65°19′	1901–1990	ORNL
Isla Gaufo	43°34′	74°45′	1908–1989	D. M. Chile
Puerto Aysen	45°20′	72°40′	1930–1992	D. M. Chile
C. Rivadavia	45°48′	67°30′	1930–1990	ORNL
Río Gallegos	51°36′	69°30′	1930–1993	ORNL
Punta Arenas	53°00′	70°51′	1930–1992	D. M. Chile
Ushuaia	54°48′	68°18′	1930–1996	ORNL

Source: ORNL: The Global Historical Climatology Network. Oak Ridge National Laboratory, Department of Energy, U.S.A.

D. M. Chile: Dirección Meterorológica de Chile.

regressions were estimated for each series and the slope of the line is indicated for the seasonal and annual means (Figures 4 and 5).

From 1930 to 1989, a significant cooling trend of 1.4 °C in the annual mean temperature is observed at Puerto Montt. The cooling was more conspicuous in summer, particularly between 1945 and 1975, and almost absent in winter (Figure 4). This cooling has also been observed by Rosemblut et al. (1997) at Valdivia (39.8° S) and Temuco (38.5° S), and can be detected as north as Valparaiso at 33° S. A lowering of sea surface temperature at the latitudinal belt of 30–42° S has been suggested by Aceituno et al. (1993) as a forcing mechanism for this cooling. This lowering of temperature along the Chilean coast only seemed to occur at the lower troposphere below 2 km level, as reported by Aceituno et al. (1993) from their analyses of upper air temperature at Puerto Montt and Quinteros (33° S).

Mean annual temperature at Bariloche, at a similar latitude to Puerto Montt but east of the Andes (Figure 2), show no significant trend (the best-fit line is slightly positive) during the interval 1930–1990. A cooling from 1950 to 1975, similar to the one documented at Puerto Montt, is also observed at Bariloche, but it was more subdued than on the western side of the Andes. After 1976 warmer temperatures were recorded at Bariloche. At 41° S, the Andes reaches an average elevation of 2000 m, separating the hyper-humid climates along the Pacific coast from the drier and continental climates on the eastern Patagonian plateau. Incursions of subtrop-
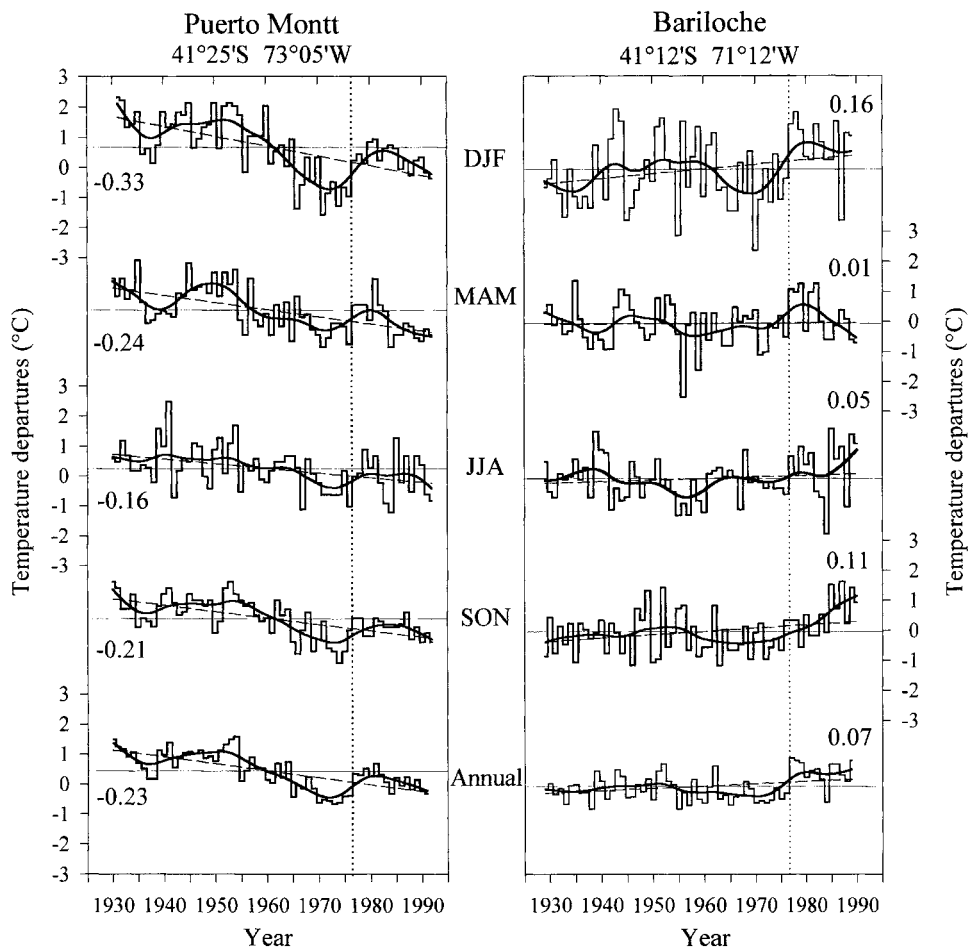
Figure 4. Comparison of seasonal, summer (December to January), fall (March to May), winter (June to August), spring (September to November), and mean annual (April to March) temperature fluctuations between Puerto Montt (left) and Bariloche (right). To emphasize the low-frequency variability, the temperature records have been smoothed with a cubic spline (Cook and Peters, 1981) designed to reduce 50% of the variance in a sine wave with a periodicity of 15 years (solid line). For the interval 1930–1990, dashed lines represent linear trends. Trends per decade are numerically indicated for each seasonal or annual mean. The simultaneous rise in summer and fall temperatures in both stations during the mid-1970s is indicated by a vertical dotted line.

ical warm air masses of continental origin in summer are common on the eastern slopes of the Andes at the latitude of Bariloche (Taljard, 1972).

At southern latitudes, a definite warming trend appears in the records, both on the Pacific and the Atlantic coasts (Figure 5). This warming is more pronounced in summer, particularly at Río Gallegos, where a warming of 2.5 °C has been recorded from 1931 to 1990. At higher latitudes the warming increases with latitude, particularly at the eastern side of the Andes (Hoffman, 1990; Rosembluth et al., 1995,
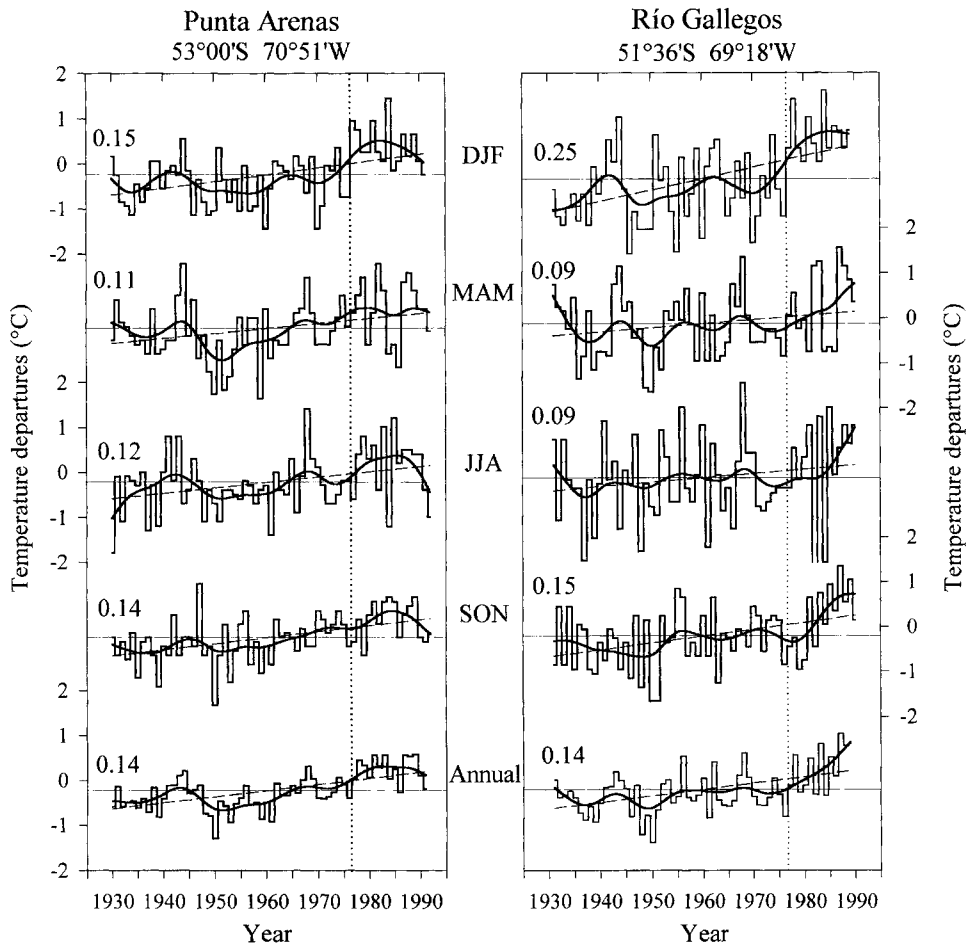
Figure 5. Comparison of seasonal and mean annual temperature fluctuations for Punta Arenas and Río Gallegos (for explanations see Figure 4).

1997). The warming at higher latitudes during the recent years is very pronounced on the Antarctic Peninsula (King, 1994), and is the cause of the extensive ice retreat in the region (Doake and Vaughan, 1991). A pronounced cooling in 1991–1992 in the Punta Arenas record, particularly during the winter months, coincides with the Pinatubo and Cerro Hudson eruptions in June and August of 1991, respectively (Rosenblüth et al., 1997).

The climatic change around 1976 is a well-established feature in the climate literature (Ebbessmeyer et al., 1991; Graham, 1994). It is also present in the Southern Oscillation Index as a change to persistent negative values for a decade or more (Trenberth, 1990). Temperatures along the Chilean coast have been unusually warm since 1976 compared to the past 80 years (Rosenblüth et al., 1997). Seasonal means from stations in southern South America show that the climatic change at

1976 was much more marked in summer than in any other seasons. The summer warming after 1976 is largely responsible for the positive trends recorded at the northern stations east of the Andes and in less degree for the stations located at higher latitudes (Figures 4 and 5).

3.2. SPATIAL TEMPERATURE PATTERNS

We used Empirical Orthogonal Function (EOF) analysis for compressing the inter-correlated set of temperature records and extracting orthogonal linear combinations that capture the maximum proportion of initial variance in the temperature data set for the southern Andes. An N × L matrix, containing L variables and N observations, may be represented as a linear combination of L EOFs projected upon L principal components (PCs). The variance explained by each EOF-PC pair is given by L eigenvalues (Richman, 1986). A widely used method is the Varimax rotation of EOFs, which yields statistically more stable patterns than the conventional EOF analysis (von Storch, 1995). Various criteria have been proposed to judge how many EOFs should be retaining as part of the climatic signal. The first three EOFs, showing eigenvalues larger than 1, were considered in this analysis.

The first EOF, capturing 45.4% of the annual temperature variability in southern South America, displays the highest loadings over northern Patagonia (37°–43° S) west of the Andes (Figure 6). This EOF encompasses the variability in temperature for the temperate Mediterranean climate with winter rains along the Pacific coast. The second EOF, which explains 21.7% of the total variance in annual temperature variations, represents north-south differences with the highest positive loading over southern Patagonia and Tierra del Fuego (Figure 6). Although largely associated with the stations south of 50° S, the second EOF loadings remain above 0.6 values along the eastern side of the Andes as far north as 40° S. This pattern represents a mixture of colder climates with rainfall well distributed throughout the year on the coastal Pacific southern sites and much drier sites on the lee side of the Andes. The third EOF, explaining 8.9% of the variance, is mainly related to the stations along the Atlantic coast north of 42° S (Figure 6). This pattern centered at above 38° S represent the coastal Atlantic pattern, characterized by dry, temperate climates.

The three leading PCs are displayed in Figures 7–9, together with some temperature records from stations located in the areas of larger PC eigenvalues. All three PCs contain both inter-decadal and inter-annual variance. Note that inter-annual variance was larger before 1960, mainly for PC1 and PC2, at times when temperature data are less reliable. The PC1 shows warmer conditions during the 1940s and 1950s, followed by a cold period from 1964 to 1975, and a recovery to warmer conditions in the 1980s (Figure 7). In contrast to PC1, PC2 is characterized by a steady warming trend that starts in the late 1940s (Figure 8). PC3 does not show any significant long-term trend in annual temperatures during the 20th century (Figure 9).
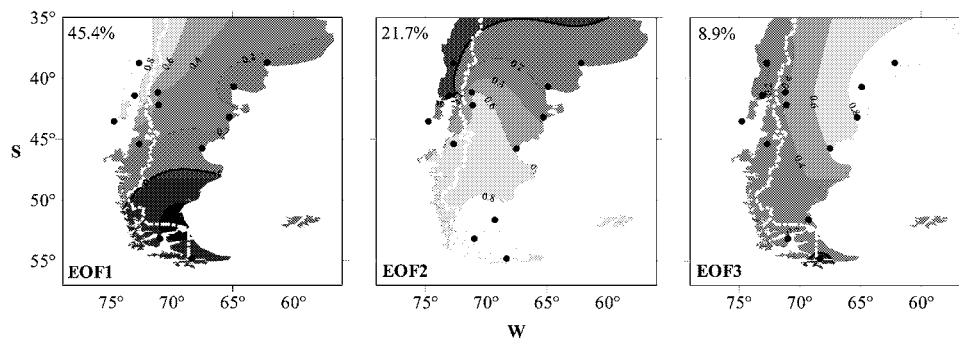
Figure 6. The three leading EOFs of annual temperature anomalies (1930–1990) in southern South America. The variance explained by each spatial pattern is indicated in the upper left corner. Circles indicate station locations.

Our results are consistent with those presented by Rosemblüth et al. (1997) in their analysis of the recent temperature variations in southern South America. Over the subtropical Chilean coast (our EOF1), they reported a marked cooling from the 1950s to the 1970s. In the south, between Puerto Aysen and Ushuaia (54° S), a steady warming beginning in the 1950s and leveling off in the 1980s was documented by the authors. According to Rosemblüth et al. (1997), most of the warming occurred in the southern sector, as it is shown in our analysis by the largest eigenvalues related to the southernmost stations (Río Gallegos, Punta Arenas and Ushuaia).

3.3. DECENNIAL AND INTER-ANNUAL VARIABILITY IN THE INSTRUMENTAL RECORDS

Recent efforts to improve our understanding of the natural climatic variability have included a growing focus on interactions between inter-annual (ENSO) and lower frequency decade- to century-scale fluctuations in climate. Singular spectral analysis (SSA, Vautard and Ghil, 1989) was use to investigate the nature and structure of climatic variability on inter-annual to decennial time scales present in the three leading modes of temperature variations in southern South America. SSA is basically a statistical technique related to EOF analysis to determine oscillatory modes in the time space. Quasiperiodic signals appear as pairs of degenerate eigenmodes and their corresponding eigenfunctions in the time domain are in quadrature with each other (Vautard and Ghil, 1989). Low frequency variability is identified in PC1 and PC2 as trends and oscillations with periods longer than 30 years (Figure 10a). The low frequency variability in RC1 (the reconstructed component from SSA on PC1), which represents more than 50% of the total variance, presents the well documented long-term behavior observed over the northern Chilean stations on the Pacific coast with positive values until late 1950s followed by negative values to late 1980s with a minimum around 1970–1975. The low frequency variability in RC2 (43.05% of the variance) is identified as a positive trend
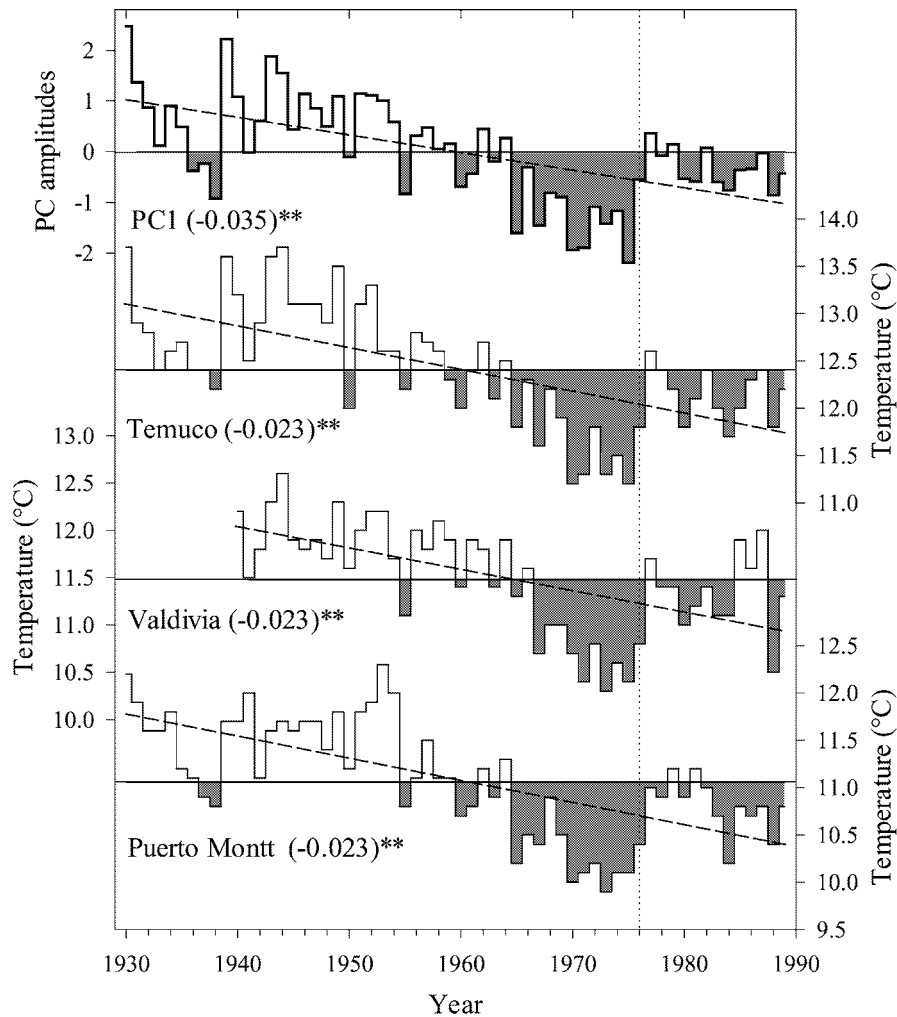
Figure 7. Variations in amplitude of PC1, corresponding to the first EOFs in Figure 6, during the interval 1930–1989. The PC1 scores are associated with the meteorological stations located in the northern sector of the southern Andes along the Pacific coast. Temuco (38°45′ S, 72°38′ W), Valdivia (39°36′ S, 73°06′ W), and Puerto Montt (41°25′ S, 73°05′ W) share a similar pattern of annual temperature variability to PC1. For the interval 1930–1989, dashed lines represent linear trends. Trends per decade are numerically indicated for each record. The simultaneous rise in annual temperatures during the mid-1970s is indicated by a vertical dotted line. Two asterisks (**) indicate linear trends statistically significant at the 99.0% confidence level (*t*-test).

starting around 1950 (Figure 10a). Both low-frequency components are negatively correlated ($r = -0.47$), but they are not significantly related due to high autocorrelations in the series (Bretherton et al., 1999). No low-frequency component, longer than 30 years in length, was detected in PC3.
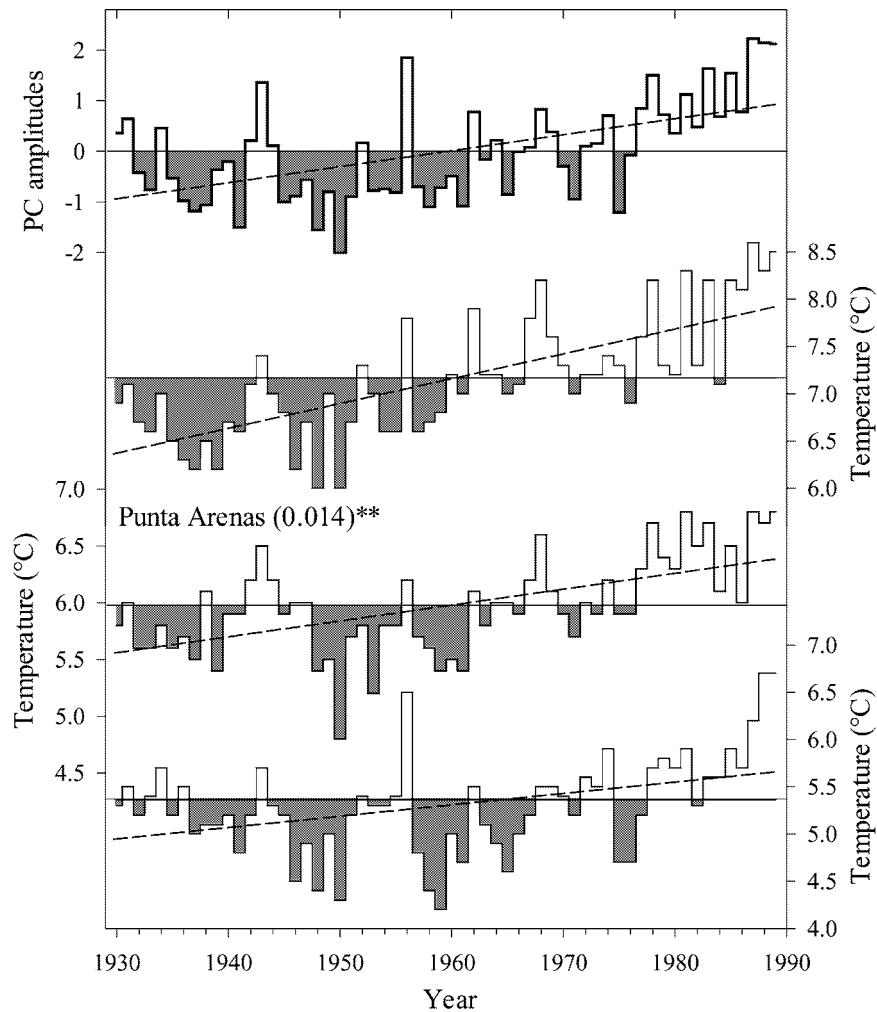
Figure 8. Variations in amplitude of PC2 (corresponding to the second EOFs in Figure 6) compared with the annual temperature records from Río Gallegos (51°36′ S, 69°30′ W), Punta Arenas (53°00′ S, 70°51′ W), and Ushuaia (54°48′ S, 68°18′ W). See Figure 7 for explanation.

Inter-decennial (11–29 years) variability was present in the three leading modes of temperature variability. The inter-decennial oscillations in RC1 and RC2 (the reconstructed inter-decennial components from SSA on PC1 and PC2, respectively) capture 9.8% and 13.2% of the annual temperature variability, respectively (Figure 10b). They display their highest spectral peaks between 12 and 17 years. The inter-decennial mode of variability is more manifest in PC3, explaining 40.06% of the total variance in temperature variations over the north Atlantic coast. An interesting feature that emerges from this comparison is the positive correlation ($r = 0.53$) between the inter-decennial modes of variability in RC1 and RC2. This
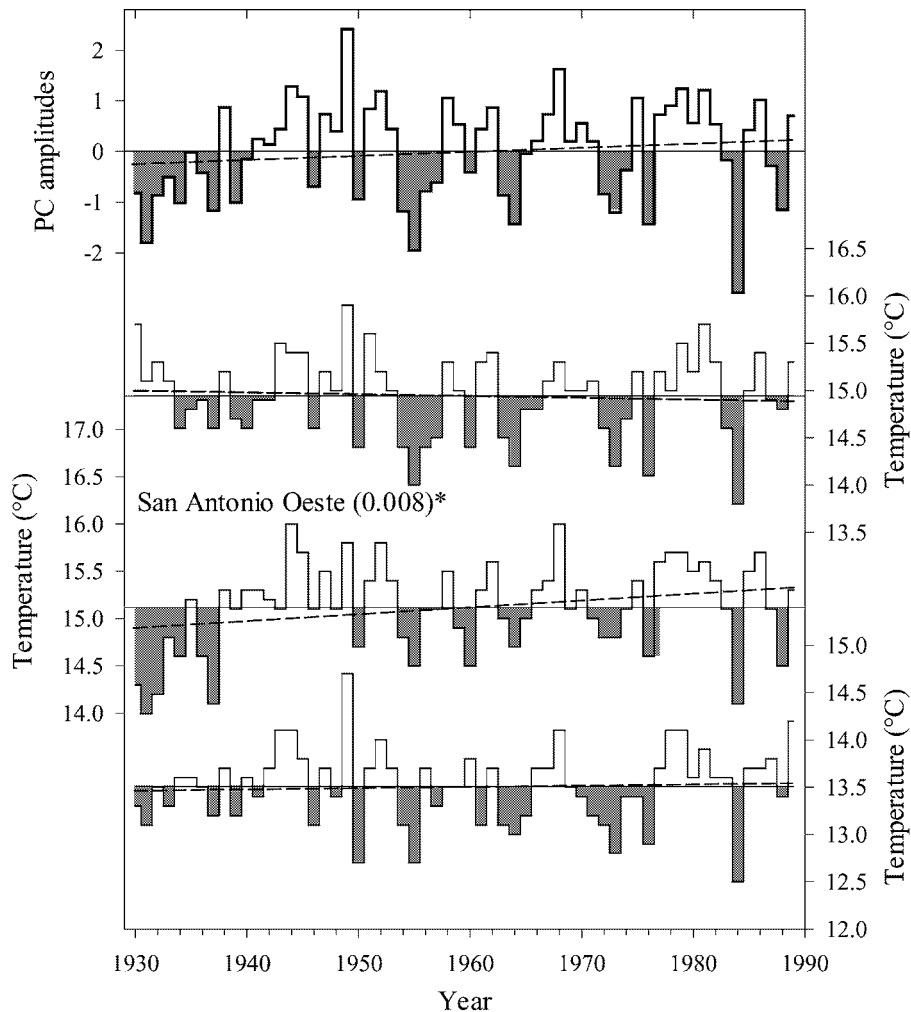
Figure 9. Variations in amplitude of PC3 (corresponding to the third EOFs in Figure 6) compared with the annual temperature records from Bahía Blanca (38°42′ S, 62°12′ W), San Antonio Oeste (40°44′ S, 64°57′ W), and Trelew (43°13′ S, 65°19′ W). See Figure 7 for explanation. One asterisk (*) indicates linear trends statistically significant at the 95.0% confidence level (*t*-test).

relationship is statistically significant at the 95% confidence level (accounting for the autocorrelation in both series the effective number of degrees of freedom is $N_{ef}^{*} = 14$, Bretherton et al., 1999), suggesting common forcings of temperature decennial variability in the northern and southern sectors of the Andes.

The inter-annual modes of temperature variability for RC1 and RC2 are also positively correlated (Figure 10c). For this comparison, the correlation coefficient ($r = 0.52$) between these series is statistically significant at the 99% confidence level ($N_{ef}^{*} = 56$), due to the low first-order autocorrelation in the inter-annual time series. Based on these results, we suggest that the north-south temperature differ-
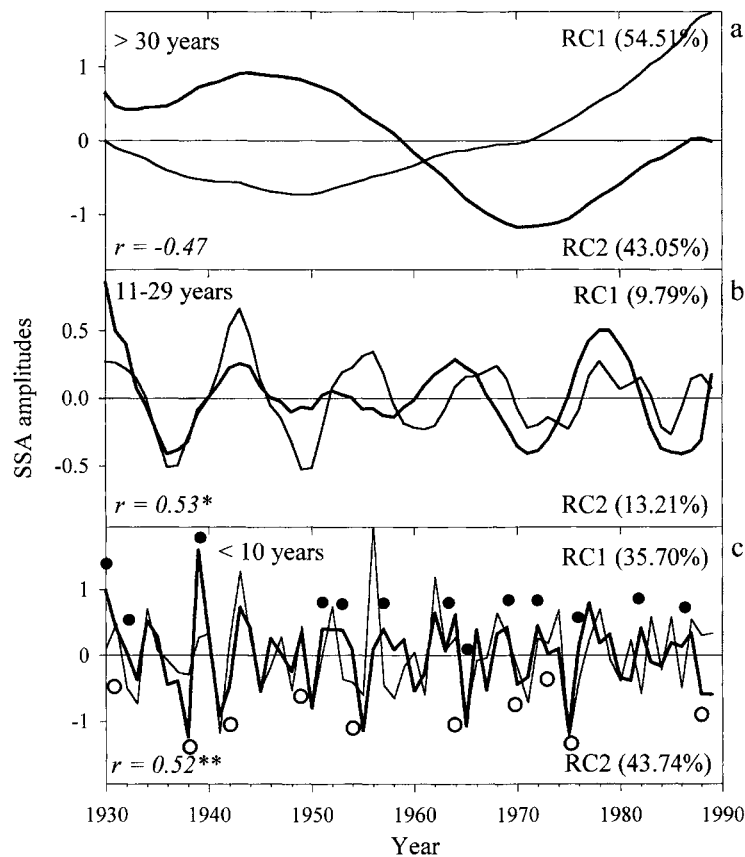
Figure 10. Singular Spectral Analysis (SSA) decomposition of PC1 (thick line) and PC2 (thin line) in wavelengths (a) longer than 30 years, (b) between 11 and 29 years, and (c) shorter than 10 years. Percentages of the original variance contributed by each of the reconstructed component (RC1 and RC2) from SSA are indicated in the upper and lower right corners of the figures, respectively. In the lower left corners, *r* is the Pearson 's correlation coefficient between the RC1 and RC2 series. In (c), solid (●) and empty (O) circles indicate warm and cold El Niño-Southern Oscillation events according to Diaz and Kiladis (1992). One (*) and two (**) asterisks indicate correlation coefficients statistically significant at the 95.0% and 99.0% confidence levels.

ences across the southern Andes during the 20th century are largely modulated by low frequency components of climate. In contrast to the long-term oscillations, decennial and inter-annual variability in temperature across the southern Andes appear to be influenced by similar regional and hemispheric climatic forcings. We observed, for instance, that 12 from the 13 warm El Niño-Southern Oscillation events listed by Diaz and Kiladis (1992) for the interval 1930–1990, are coincident with positive departures in the RC1 and RC2 inter-annual climatic components. No significant correlations were observed between the inter-decennial or inter-annual modes of climate variability along the Atlantic coast (RC3) and those recorded for the northern and southern sectors of the southern Andes.

4. Tree-Ring Records

A great deal of progress has been made in increasing the number of upper eleva-
tion tree-ring chronologies across the southern Andes since the Boninsegna et al.
(1989) paper on treeline records from Tierra del Fuego. This work has involved the
development of more than 90 chronologies from collections of *Nothofagus pumilio*,
the dominant subalpine tree in the Andes of Chile and Argentina (Villalba et al.,
1997; Aravena et al., 2000; Lara et al., 2001; Roig et al., 2000; Schmelter, 2000;
Wolodarsky-Franke et al., 2000; Masiokas et al., 2001). These new collections have
increased both the spatial coverage (ca. 35°35′ to 55° S) and the temporal span of
upper-elevation records across the southern Andes.

Two tree-ring records from *Nothofagus pumilio* were selected to reconstruct
the past variations in the PC1 pattern associated with the temperature variations
in the northern sector of the southern Andes (see Table II, and the section on
Methods for generating the tree-ring reconstructions for details on the chronolo-
gies and selection procedures). The COV7-8 is a composite chronology resulting
from merging sites COV7 and COV8, previously described as independent records
in Villalba et al. (1997). These sites are located along an elevational gradient in
the Mount Tronador area (41°09′ S, 71°49′ W) at 1410 m and 1300 m elevation,
respectively. Trees included in the CDL2 chronology were sampled from an old
stand of single-stemmed trees at 1500 m elevation on the slopes of Cerro Diego de
León (41°12′ S). This chronology was first described in Villalba et al. (1997), but
the version presently used in this paper included new samples recently collected
by Schmelter (2000). The sample sizes for COV7-8 and CDL2 average around 40
and 55 ring-width measurements per year back to 1800, 25 and 20 in the interval
1700–1800 and 12 and 10 in the 1600–1700 period, respectively.

Three records were used to reconstruct the temperature variations in the south-
ern sector of the southern Andes. The CTI-CTM is a composite record of two
nearby *Nothofagus pumilio* chronologies around Lago Cochrane (47° S, 10′ S),
Chile. CTI and CTM at 1060 and 1100 m elevation, respectively, are located on
the western slope of the Andes, and consequently, in wetter sites than the other two
records. The AGN-GNV1-2 composite chronology results from the combination of
three individual records located within the Río Narvaéz catchment (48° S), ranging
between 930 and 990 m elevation. A large part of the valley is still covered by
the Narváez glacier, and only the lower 7–8 km are now free of ice. Finally, the
GBP chronology was developed from *Nothofagus pumilio* trees growing on the
Holocene moraines of Piedras Blancas Glacier at 600–650 m elevation. At the
latitude of GPB (49°21′ S), the forest is reduced to a narrow band of 5–50 km
wide confined between the Southern Patagonian Icefield and the Patagonian steppe.
Site GBP was sampled in 1998 and re-visited in 2000. The sample sizes for the
southern chronologies average between 30 and 55 ring-width measurements per
year back to 1800, 20 in the interval 1700–1800 and >10 in the 1600–1700 pe-
riod. No significant relationships were found between PC3 and the *Nothofagus*
chronologies.

Table II
Site characteristics for the tree-ring chronologies included in the composite chronologies

Composite chronology	Sites	Code	Latitude (°S)	Longitude (°W)	Elevation (m)	Aspect	Source
COV7–8	Castaño Overo 7	COV7	41°09'	71°49'	1410	E	Villalba et al., 1997
	Castaño Overo 8	COV8	41°09'	71°49'	1300	SE	Villalba et al., 1997
CDL2	Cerro D. de León	CDL2	41°12'	71°40'	1500	N–NW	Villalba et al., 1997 Schmelter, 2000
CTI-CTM	Cerro Tamango Inf.	CTI	47°10'	72°30'	1060	S–SW	Wolodarsky et al., 2000
	Cerro Tamango Med.	CTM	47°10'	72°30'	1100	S–SW	Wolodarsky et al., 2000
AGN-GNV1–2	Puesto Miraflores	AGN	48°28'	72°09'	1039	N–NE	Masiokas et al., 2001
	Glaciar Narváez 1	GNV1	48°28'	72°15'	960	N–NE	Masiokas et al., 2001
	Glaciar Narváez 2	GNV2	48°28'	72°15'	930	N–NE	Masiokas et al., 2001
GPB	Gl. Piedras Blancas	GPB	49°21'	72°58'	650	E	Masiokas et al., 2001

Table III

Pearson's correlation coefficients between the composite chronologies across the southern Andes. The interval used for comparison is 1630–1991 ($n = 362$ years, effective degrees of freedom $N^*_{ef} = 147$ years). See Table II for chronology code definitions. All correlation coefficients are statistically significant at the 99.99% confidence level

	CDL2	CTI-M	AGN-GNV1–2	GBP
COV7–8	0.620	0.334	0.388	0.311
CDL2	–	0.340	0.377	0.260
CTI-M		–	0.606	0.439
AGN-GNV1–2			–	0.449

Table III shows the correlation patterns among the composite chronologies from the northern and southern sectors of the southern Andes. The correlation coefficients remain statistically significant over the entire southern Andes, reflecting the temperature-sensitive nature of the selected chronologies. As expected, correlation coefficients between chronologies decrease as distance between sites increases.

Figures 12 and 13 show the resulting tree-ring chronologies for the northern and southern sectors of the southern Andes, respectively. Smoothing splines have been superimposed on the chronologies to emphasize fluctuations longer than 25 years in duration. Both chronologies from the northern sector start in the mid-16th century, but they are shown in Figure 12 since 1600. Sample size information for each chronology is also included at the bottom of each figure. Variations in sample size have been used to correct the variance of the mean chronology due to changes in sample sizes in a theoretically correct way (Osborn et al., 1997).

4.1. STANDARDIZATION METHODS

Standardization is the process of removing variability in tree rings that is not related to climate such as tree ageing or forest disturbances. The substantial increase in sample replication over the chronologies used in Villalba et al. (1997) and the development of composite chronologies, which include more than 50 samples in most cases, has allow us to standardize the *Nothofagus* tree-ring series using the regional curve standardization (RCS) method. This much more conservative method of standardization allows for the preservation of low-frequency variance in excess of the length of the individual segments used in creating the tree-ring chronology (Briffa et al., 1992, 1996). The RCS method estimates a single mean growth curve that represents the intrinsic trend in radial growth as a function of age. In order to determine the biological age of the rings it is necessary to include a large number of samples to capture the real nature of the biological trends and estimate

for each sample the number of missing years to the pith. However, it appears that the RCS method is not sensitive to this latter uncertainty, particularly for species with relatively little trend during the period of juvenile growth (Cook et al., 2000), as occurs in *Nothofagus pumilio*.

Figure 11 shows the mean ring-wind series resulting from averaging all the individual series of radial growth from the northern and southern sectors of the southern Andes, after they have been aligned by biological age. RCS curves for individual chronologies are very similar to their regional means. Consequently, only the RCS regional curves, together with the sample sizes as a function of years from the pith, are shown in Figure 11. A systematic decline of ring width with age is recorded for the chronologies located in the northern sector, whereas a more noticeable decline is observed in the southern sector for samples of length above 250 years. However, this more marked decline of the mean value function might be an artifact due to the abrupt decrease in the number of measurements after year 250. The mean growth series shown in Figure 11 are not used to standardize the individual tree-ring series because they are noisy. Instead, simple theoretical curves fit to the mean series were used to detrend and standardize all of the individual ring-width series in each chronology.

To assess the temporal variability in the strength of the common signal, we calculated running series of average correlation (Rbar) and expressed population signals (EPS) statistics for the chronologies (Figure 14). Rbar is the mean correlation coefficients for all possible pairings among tree-ring series from individuals cores, computed for a specified common time interval (Briffa, 1995). We used a 50-year window with an overlap of 25 years between adjacent windows. For the chronologies in the northern sector of the southern Andes, the Rbar statistic oscillates between 0.22–0.55 over most of the past 400 years (Figure 14). Similar values of Rbar were recorded for the chronologies in the southern sector (Figure 14), but a conspicuous deterioration in precision before 1650 was observed in the southern chronologies due to declining in sample size.

The positive response of *Nothofagus pumilio* to increasing temperature is a typical pattern for trees near upper treeline and reflects the direct influence of temperature on physiological processes related to tree growth (Tranquilini, 1979, Körner, 1999). It has been previously noted by Villalba et al. (1997), that individuals of *Nothofagus pumilio* which are severely limited by temperature integrate the effects of low-frequency thermal variations (air and soil temperatures, insolation) for all seasons, and their growth correlates best with annual temperatures (Figures 15 and 16). Indeed, we found that the regression models are more efficient when upper-elevation *Nothofagus pumilio* chronologies are used as predictors of annual instead of seasonal temperature variations. In the cold environments at upper treeline, severe winter storms dry the parts of the trees that emerge from snow. This loss of biomass is reflected in a reduction of the rate of tree growth during the following growing seasons. In consequence, mean annual temperatures, which integrate
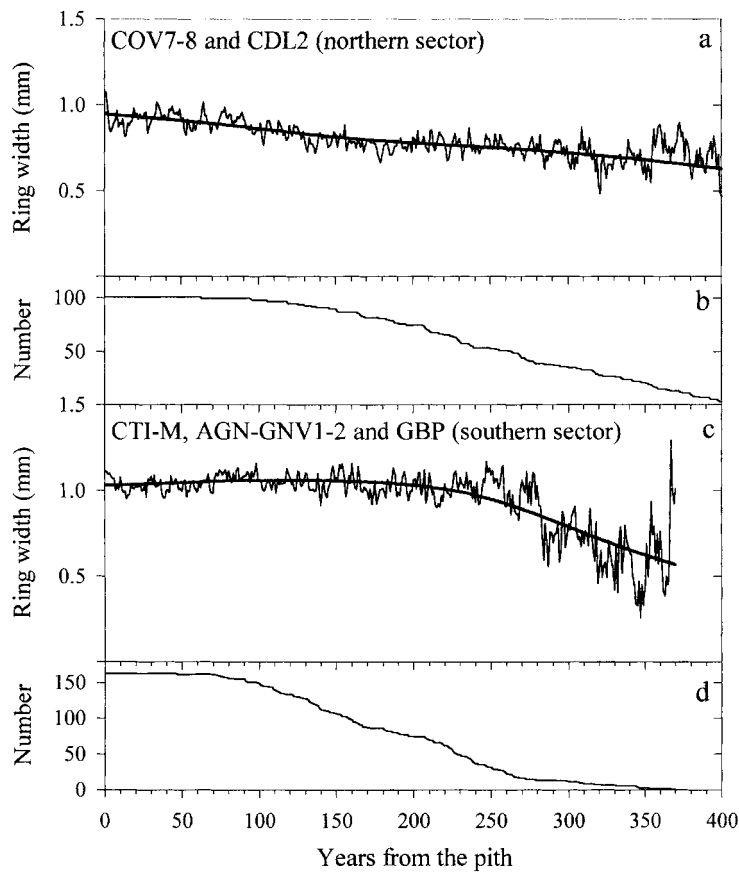
Figure 11. The Regional Curve Standardization (RCS) lines used for standardization the northern (a) and southern (c) chronologies from *Nothofagus pumilio* in the southern Andes. The smooth thick curves in (a) and (c) represent simple theoretical growth curves fitted to the mean series. The number of measurements per year is indicated for the northern and southern chronologies in (b) and (c), respectively.

summer warmth and winter severity, rather seasonal changes in temperatures, were chosen as predictans in the reconstructions.

The signal strength in a mean chronology may be gauged by calculating the degree to which it represents the hypothetical (noise-free) chronology, or a chronology that has been infinitely replicated (Briffa, 1995). This signal strength is measured in the individual chronology by the statistic expressed population signal (EPS). The dotted line in Figures 14b,c delineate a threshold of 0.80 in the running EPS. The northern and southern groups of chronologies have EPS in excess of 0.80 as far back as the 1625 and 1675, respectively, and marginally worse before these dates. Based on these measurements of the strength of the common variation in the chronologies, we established that the northern and southern chronologies are reliable for climate reconstructions back only to 1625 and 1675, respectively.
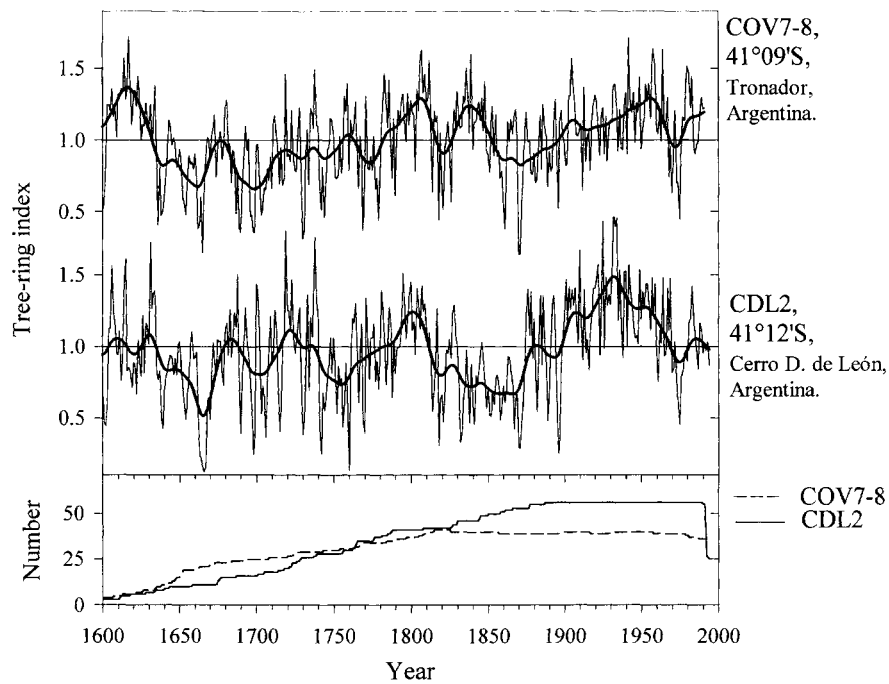
Figure 12. The COV7-8 and CDL2 composite chronologies standardized using the RCS curves shown in Figure 11a. Sample sizes for the chronologies are indicated in the lowest diagram.

4.2. CLIMATE-TREE GROWTH RELATIONSHIPS

To identify month-to-month relationships between climate and *Nothofagus* tree growth at upper treeline, we computed correlations between the chronologies and monthly mean temperatures (Fritts, 1976; Blasing et al., 1984). The statistical association between ring indices and each monthly temperature variable was examined over the common period for the chronologies and the instrumental record. As radial growth is influenced by climatic conditions several months before ring formation (Fritts, 1976), we included a temporal span covering both the previous and the current growing seasons. Consequently, correlations between ring width and temperature data were calculated for 20 months, starting with October of the previous growing season and ending with May of the current growing season.

For comparisons between temperature patterns and radial growth, we create regional means by averaging the monthly temperature values from the three meteorological stations most strongly associated with PC1 and PC2. To give a similar weight to each of the temperature record in the regional mean, data were converted to standard deviations from the monthly temperature means for each station and then averaged among stations. Temperature records for the northern sector of the southern Andes include the stations of Temuco, Valdivia and Puerto Montt
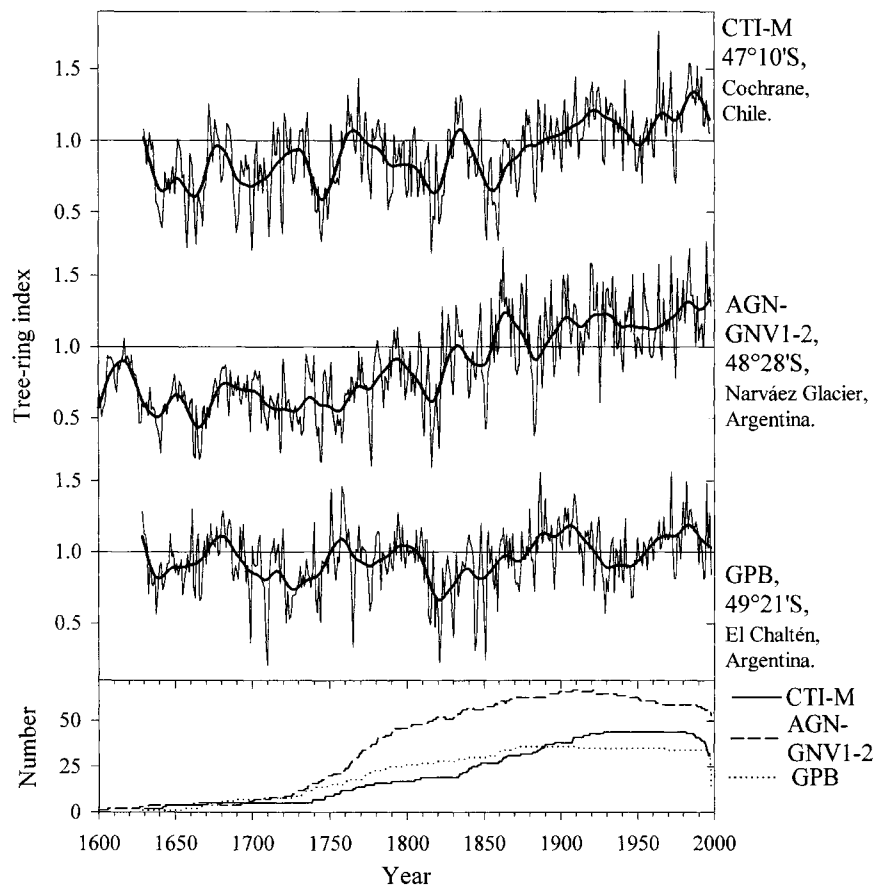
Figure 13. The CTI-CTM, AGN-GNV1-2 and GPB composite chronologies standardized using the RCS curves shown in Figure 11c. Sample sizes for the chronologies are indicated in the lowest diagram.

(Figure 7), whereas the southern regional average consist of the temperature records from Río Gallegos, Punta Arenas and Ushuaia (Figure 8).

Figure 15 shows the correlations between the regional temperature record from the northern sector and the two indexed ring-width chronologies (COV7-8 and CDL2) used in the reconstruction of the PC1 temperature pattern. Significant positive correlations are observed for most months over the comparison interval. Statistically significant correlations occur mainly during both growing seasons, whereas a decline is recorded around May in both the previous and current growing seasons. In contrast to the northern sector chronologies, growth at the southern sector is more strongly correlated with previous summer and late winter-early spring temperatures (Figure 16). Correlations with current growing season months are either barely significant or not significant. Correlations approach zero values in April of both current and growing season, precisely one month earlier than in the northern sector.
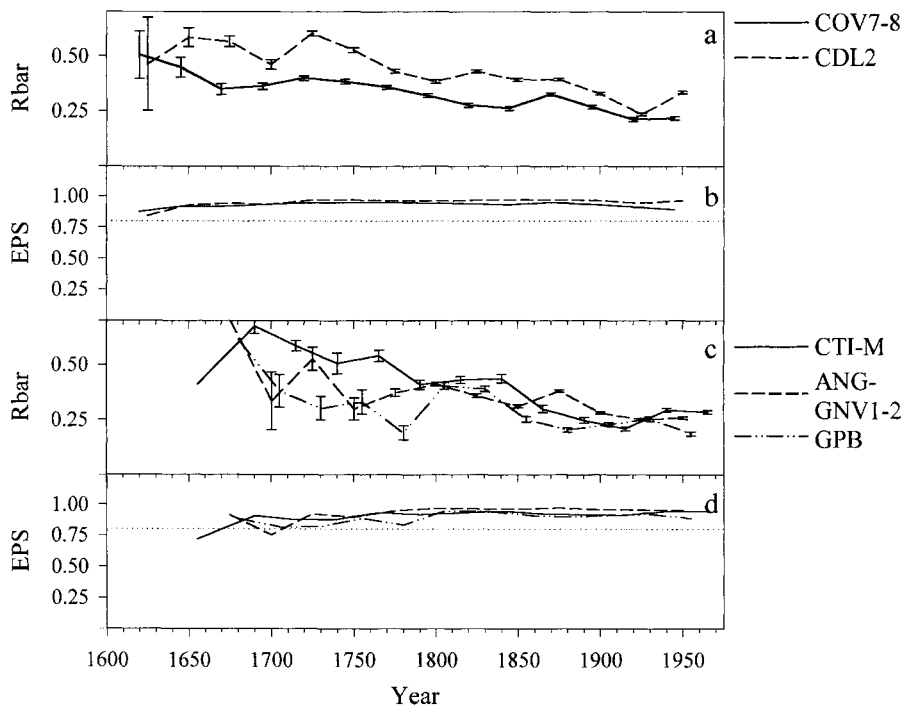
Figure 14. The Rbar and EPS statistics for the northern ((a) and (b)) and southern ((c) and (d)) composite chronologies. These statistics are a measure of the strength of the common signal among the individual series. The moving window used for computing Rbar and EPS statistics is 50 years with an overlap of 25 years between adjacent windows. For Rbar, the vertical bars represent the 2 standard error limits. The dotted lines in (b) and (d) delineate a threshold of 0.80 for the EPS.

4.3. METHODS FOR GENERATING THE TREE-RING RECONSTRUCTIONS

In an attempt to maximize the temperature signal, the *Nothofagus pumilio* tree-ring chronologies available for southern Andes were subjected to a statistical screening prior to use in the reconstruction procedures. Those chronologies well replicated (>5 samples) to the year 1650 and with the strongest correlation for the overlapping 1930–1989 interval with the PC records representing the annual temperature patterns across the southern Andes (Figures 7 and 8) were selected to use in the regression analyses. The screening criterion for selecting the chronologies as predictors was the 0.05 probability level of the Pearson correlation coefficient with $n - 2$ degrees of freedom, in this case 58 for the 1930–1989 comparison period. Table IV shows the correlation probability levels between the chronologies and the PC temperature patterns. We used regression on principal components (Cooley and Lohnes, 1971) to orthogonalize the inter-correlated set of chronologies (predictors) and reduce the dimension of the regression analysis by eliminating the high-order eigenvectors that account for very little variance. Only eigenvectors showing eigenvalues >1 were retained in the model.
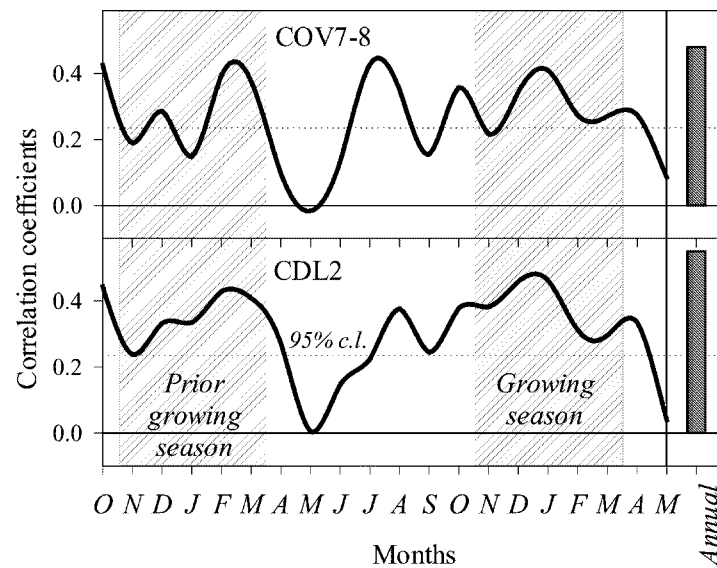
Figure 15. Correlation functions, based on standard chronologies, showing the correlations between mean monthly temperatures and ring width indices of *Nothofagus pumilio* for the COV7-8 and CDL2 chronologies. Correlation coefficients are for standardized ring width against the average of normalized departures of monthly mean temperatures from Temuco, Valdivia and Puerto Montt, for the period 1930–1989. Correlation coefficients between annual (April to March) temperature variations and ring width indices are shown on the right side of the diagrams. Positive correlation indicates that above-average tree growth is associated with above-average values of the climatic variable. Coefficients greater than 0.25 (dotted lines) are significant at the 95% confidence level.

Climatic conditions in a given year affect growth in the same year and also in the following years. It was shown in Villalba et al. (1997) that low frequency components in the radial growth of *Nothofagus pumilio* in the subalpine zone appear to be closely associated with variations in mean annual temperature. The autocorrelation function of previous temperature reconstructions with *Nothofagus pumilio* displays significant coefficients from 1- to 8-year lags. Tree growth in any particular year (t) is also influenced by growth conditions in the previous year ($t − 1$, Fritts, 1976). Consequently, annual temperature variations in the year t were modeled as a function of tree growth in the years $t − 1, t, t + 1, t + 2$, and $t + 3$. The inclusion in the regression models of additional lags did not substantially increase the percentage of total variance explained by the models. We used the Guiot's PVP criterion, a measure of the tradeoff between the goodness-of-fit of the regression and the number of predictors in the model (Guiot, 1990), to select the best-fit regression models.

Cross-validation tests were next performed for the 1930 to 1989 interval. We divided the PC records into two intervals, using the interval 1930–1969 (40 years) for the calibration and reserving the interval 1970–1989 (20 years) for verification. Then, we reversed the process selecting the 40 most recent years (1950–1989) for

Table IV

Descriptive statistics for the composite chronologies from the southern Andes

Code	No. trees	No. radii	Record period	Mean[a] sens.	Stand. dev.	Auto[b] correl.	Mean[c] RBAR	AR[d] model	Prob[e] level
Northern sector chronologies									
COV7–8	25	45	1562–1990	0.311	0.526	0.676	0.190	AR(2)	$p = 0.002$
CDL2	39	56	1546–1990	0.320	0.530	0.657	0.292	AR(3)	$p < 0.001$
Southern sector chronologies									
CTI-M	30	45	1630–1997	0.251	0.392	0.650	0.230	AR(1)	$p < 0.001$
AGN-GVN1–2	49	81	1599–1998	0.311	0.487	0.609	0.242	AR(1)	$p = 0.004$
GPB	28	74	1629–1998	0.285	0.450	0.677	0.177	AR(3)	$p = 0.002$

Mean sensitivity, standard deviation, and autocorrelation values are for standard chronologies (Cook, 1987). See Table II for chronology code definitions.

[a] Mean sens. is the mean sensitivity which is a measure of the relative changes in ring width indices from year to year and is calculated as the absolute difference between adjacent indices divided by the mean of the two indices (Fritts, 1976).

[b] Autocorrelation is the serial correlation coefficient for the chronology at a lag of 1 year (i.e., the first-order autocorrelation).

[c] Mean RBAR is the mean correlation coefficient of all replicate comparisons among the tree-ring series (Briffa, 1995).

[d] AR(n) is the autoregressive process of order n used to model the tree-ring series (Cook, 1987). The autocorrelation order n was determined by the minimum Akaike information criterion procedure (Priestley, 1992).

[e] Two-tailed probability level of the Pearson correlation coefficient between prewhitened chronologies and regional temperature patterns (PC1 and PC2) (April to March) with $n - 2$ degrees of freedom.
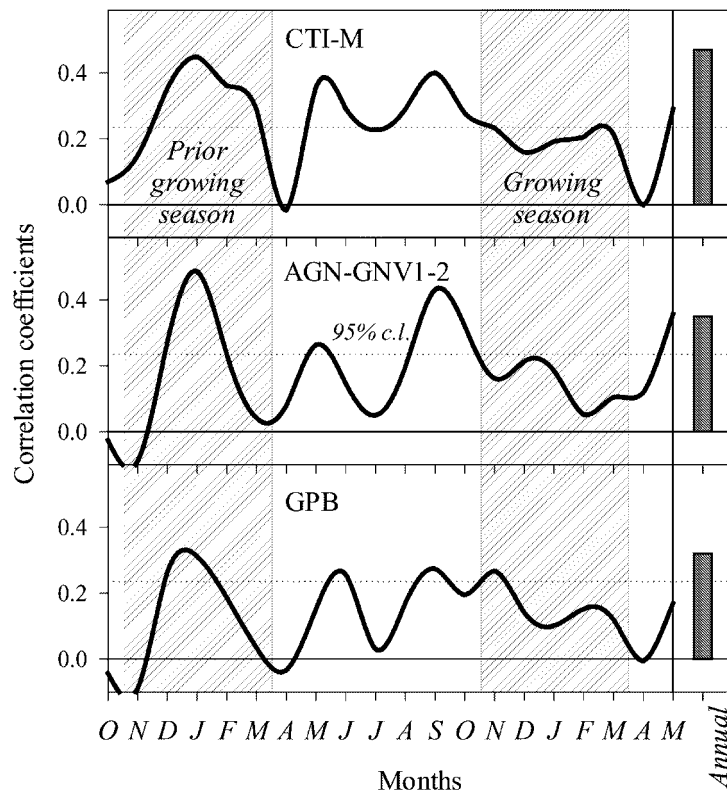
Figure 16. Correlation functions, based on standard chronologies, showing the correlations be-tween mean monthly temperatures and ring width indices of *Nothofagus pumilio* for the CTI-CTM, AGN-GNV1-2 and CDL2 chronologies. Correlation coefficients are for standardized ring width against the average of normalized departures of monthly mean temperatures from Río Gallegos, Punta Arenas and Valdivia, for the period 1930–1989. Correlation coefficients between annual (April to March) temperature variations and ring width indices are shown on the right side of the diagrams. Positive correlation indicates that above-average tree growth is associated with above-average val-ues of the climatic variable. Coefficients greater than 0.25 (dotted lines) are significant at the 95% confidence level.

the calibration and withholding the earliest 20 years for verification. The results of the regression exercises using the northern and southern groups of chronologies as predictors of PC1 and PC2, respectively, are shown in Table V. Finally, the whole 1930–1989 interval was used to derive the final regression equations, which were employed to develop the PC reconstructions. The longest calibration interval maximizes the time scale of variability against which the final regression equation could be fitted and enhances the ability of the regression model to reconstruct the low-frequency variability in the temperature patterns.

The regression equation for the annual PC1 temperature pattern explained 55% of the variance over the 1930–1989 calibration interval (Figure 17). The correlation between observed and predicted values for the independent, cross-validation peri-

Table V

Calibration and verification statistics computed for the tree-ring based reconstructions of mean annual (April to March) temperatures at the (a) northern (PC1) and (b) southern (PC2) sectors of the southern Andes; r^2_{adj}, the square of the multiple correlation coefficient adjusted for loss of degrees of freedom; r, the Pearson correlation coefficient; RE, the reduction of error statistic (Fritts, 1976)

Calibration time period	r^2_{adj}	Verification time period	r	RE
(a) Mean annual temperature for the northern (PC1) sector of the southern Andes				
1930–1969	0.27	1970–1989	0.78	+0.80
1950–1989	0.62	1930–1949	0.30	+0.46
1930–1989	0.55			
(b) Mean annual temperature for the southern (PC2) sector of the southern Andes				
1930–1969	0.26	1970–1989	0.60	+0.49
1950–1989	0.44	1930–1949	0.62	+0.61
1930–1989	0.45			

ods were significant (Table V). The reduction of error statistics is highly positive, indicating useful skill in the regressions (Gordon and LeDuc, 1981). From inspection of Figure 17, it is obvious that the reconstruction better captures the long-term than the inter-annual variations in PC1. This is consistent with our goals of using very conservative methods of standardization of the tree-ring records intended to recover the decade- to century-scale variations in temperature patterns and the large number of lags (5 years) used in the regression models.

To see how the different oscillation modes of temperature variations in PC1 were captured for our reconstruction, we performed spectral and cross-spectral analyses on the actual and reconstructed temperatures over the common 1930–1989 period using a combination of Blackman–Tukey (BTM; Jenkins and Watts, 1968) and singular spectral analyses (SSA). These results are shown in Figure 18. The power spectra show the distribution of variance as a function of frequency in each series. Although the spectral powers are very similar (Figure 18a), the coherency spectrum reveals clear differences between actual and reconstructed temperature patterns. The coherency is a measure of the relative agreement between actual and estimated temperatures as a function of frequency, and, in consequence, it can be interpreted as a series of squared Pearson correlation coefficients between series. At periods longer than 10 years, the coherency values range between 0.6 and 0.95, which indicates excellent agreement between actual and estimated temperature variations at decade- to multi decade-scales. Coherency declines abruptly for higher frequencies, reaching values above 0.6 around 5 and 3.3 years only.
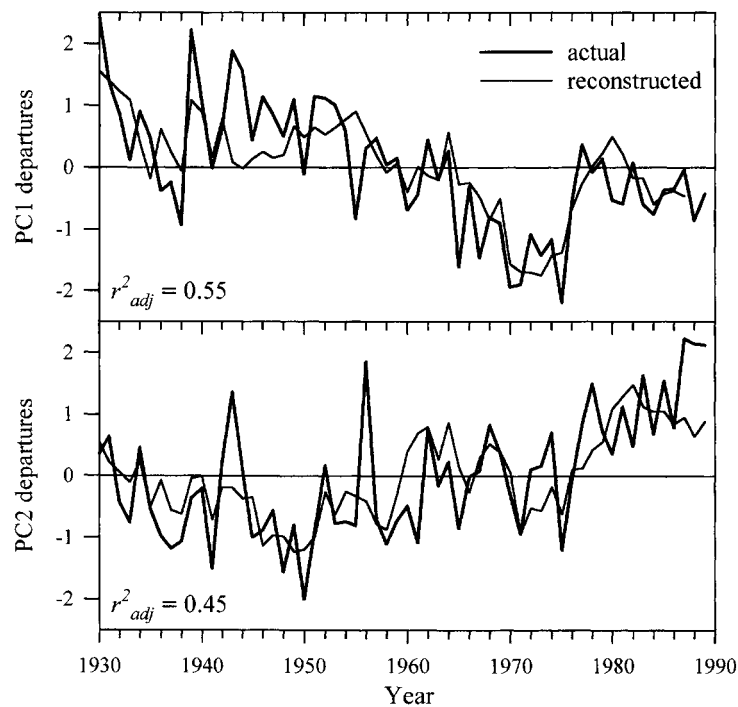
Figure 17. Actual and reconstructed mean annual temperature variations (previous April through March of the current growing season) from 1930 to 1989 for the northern (PC1) and southern (PC2) sectors of the southern Andes.

Consistent with these results, the SSA analysis (Figure 18 right) shows remarkable coincidence among the reconstructed SSA modes for the actual and estimated temperature oscillations at wavelengths longer than 30 years and between 11 and 29 years. However, due to the high values of autocorrelations in the longer time mode, only the series portraying the 11–29 year mode are significantly correlated at 99% confidence level. High-frequency variations (<10 years) are poor reproduced by the reconstruction.

Regression equations for the PC2 temperature pattern explained 45% of the total variance for the 1930–1989 calibration interval (Figure 17). The verification statistics indicate some skill in the reconstructions of PC2 pattern (Table V). Cross-spectral analysis with the instrumental data indicates that the reconstruction is more coherent with the actual temperatures at periods longer than 15 years (Figure 19). SSA shows in a different way the same basic result as the BTM cross-spectral analysis. Oscillatory modes longer than 30 years are well reproduced by the reconstructions, whereas the temperature variability at periods shorter than a decade is somewhat underestimated. Very high coherencies (>0.6) between actual and estimated temperature patterns in the low-frequency bandwidth clearly indicates that the annual reconstructions of temperature variability for the northern and southern
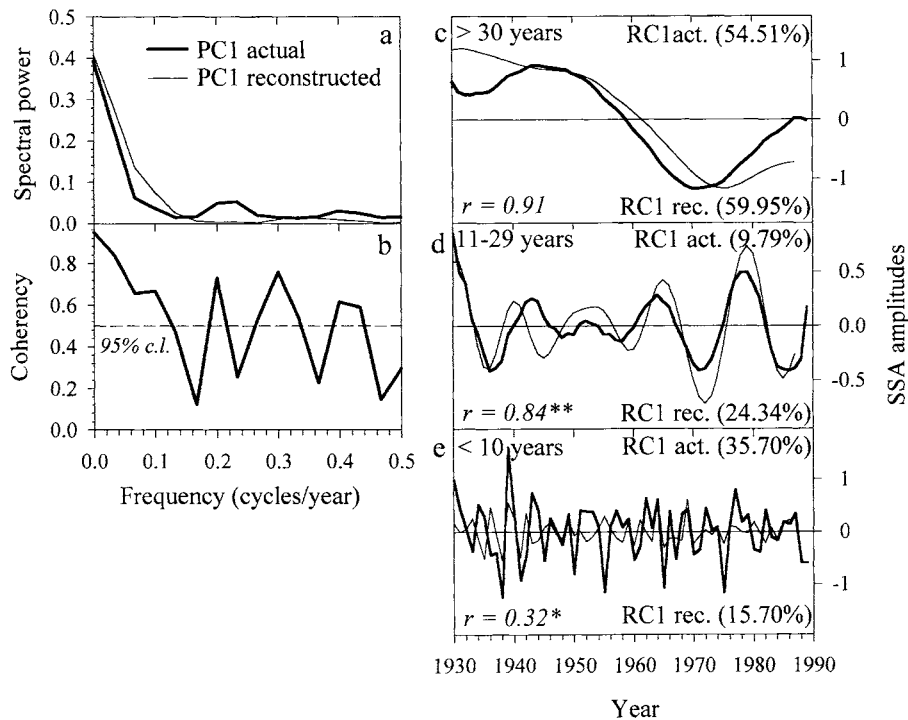
Figure 18. Blackman–Tukey (BTM) power spectra of actual and reconstructed temperature variations in the northern sector of the southern Andes estimated over the interval 1930–1989 (a). The coherency spectrum between these two records is shown in (b). Records are highly coherent at decennial-scale wavelengths longer than 10 years. Singular Spectral Analysis (SSA) decomposition of actual and reconstructed PC1 in wavelengths (c) longer than 30 years, (d) between 11 and 29 years, and (e) shorter than 10 years. Percentages of the original variance contributed by each of the actual and reconstructed waveforms are indicated in the upper and lower right corners of figures (c), (d), and (e), respectively. In the lower left corners, *r* is the Pearson's correlation coefficient between the actual and reconstructed RC1 series. One (*) and two (**) asterisks indicate correlation coefficients statistically significant at the 95.0% and 99.0% confidence levels.

sector of the southern Andes are most reliable for providing estimates of climate variability on decennial to centennial time scales. Care must be taken in deriving estimates of high-frequency natural variability from these reconstructions.

5. The Temperature Reconstructions

The PC1 reconstruction indicates that, despite relatively cool years in the late 1960s and 1970s, temperatures during the 20th century were the warmest in the context of the past 400 years (Figure 20). A secondary warm event is recorded at the end of the 18th-begining of the 19th century. Significant cold events are centered on 1650–1660, 1700 and from 1820 to 1870. The reconstructed PC1 mean for the interval
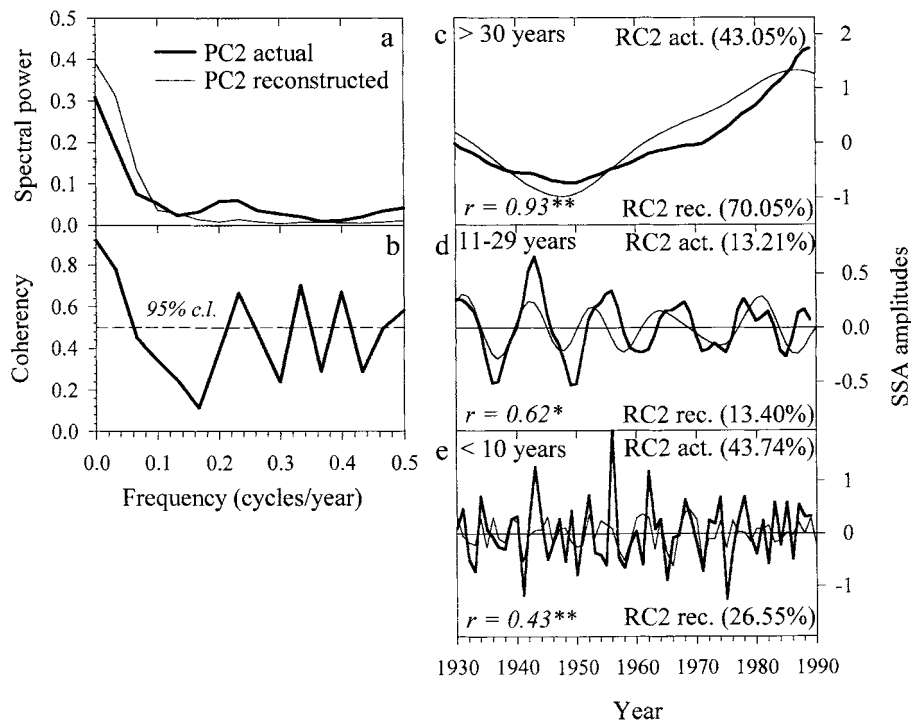
Figure 19. Blackman–Tukey (BTM) power spectra of actual and reconstructed temperature variations in the southern sector of the southern Andes estimated over the interval 1930–1989 (a). The coherency spectrum between these two records is shown in (b). Records are highly coherent at decennial-scale wavelengths longer than 15 years. See Figure 18 for further explanations.

1640–1989 departs –0.75 from the actual mean, which represents a decrease in mean annual temperature of 0.39 °C.

The reconstructed PC2 temperature pattern for the southern sector of the southern Andes shows and extended period of cold years persisting from 1640 to 1850, followed by a strong increase in temperatures peaking in the 1980s (Figure 20). The 17th, 18th and the first half of the 19th century were notably cold, particularly the 1650s and 60s, the 1690s and 1700s, the 1740s, the 1810s and the 1850s. Mean annual temperatures of the twentieth century appear to be the warmest during the past 4 centuries. The reconstructed PC2 mean for the interval 1640–1989 is –1.17 departures from the observed mean, which represents a decrease in mean annual temperature of approximately 0.64 °C.

An alternative picture of the long-term history of cold-warm periods is given by averaging the reconstructions using intervals of 10-, 25-, and 50-year. Based on a 10-year moving average, four of the five warmest periods in the northern sector occurred since 1899 (Table VI). In contrast, none of five coldest 10-year intervals occurred during the 20th century. Cold spells were frequent from 1633 to 1668, from 1694 to 1703, and from 1850 to 1872. For the southern part of the southern
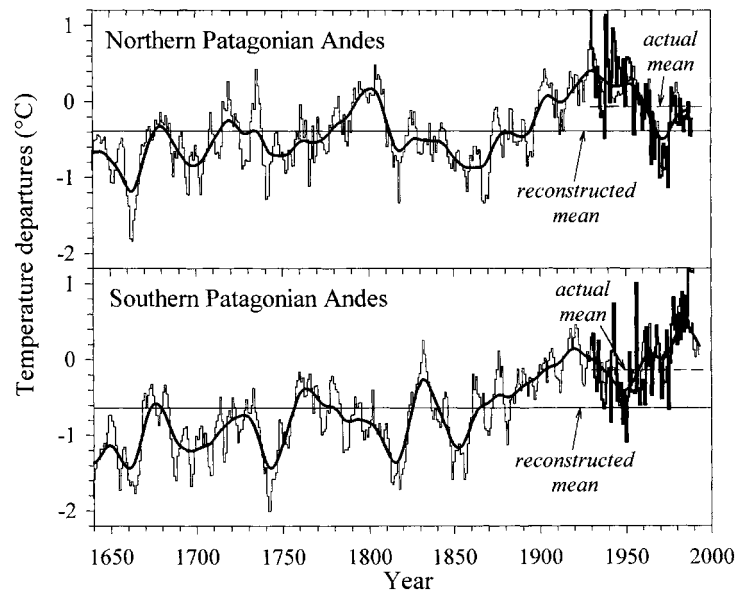
Figure 20. Tree-ring based reconstructions of mean annual temperature departures for the northern and southern sectors of the southern Andes from 1640 to 1989. To emphasize low frequency variations, the reconstructions are also shown in smoothed versions (thick line) based on smoothing the annual values with a cubic spline designed to reduce 50% of the variance in a sine wave with a periodicity of 25 years. The actual values have been superimposed in the most recent portion of the reconstructions. Both actual and reconstructed means are shown.

Andes, the four 10-year, non-overlapping positive departures all took place since 1914, whereas cold events were common from 1635 to 1667, 1738 to 1747 and from 1812 to 1857 (Table VII). In terms of the 25-year moving averages, the periods from 1918 to 1942 and 1968 to 1992 are ranked at the top among the warmest events over the past 360 years for the northern and southern reconstructions, respectively. The marked cold events during the middle 17th century, with departures of –0.95 °C in the north and –1.29 °C in the south, are also a prominent feature revealed by the 25-year moving averages. Similar patterns emerge when the analysis is extended to 50-year periods. The intervals 1915–1964 and 1944–1993 constitute the two single positive 50-year means in the northern and southern reconstructions, respectively. On this long-term scale, the coldest intervals occurred during the second part the 17th century with remarkable coolings of –0.75 °C and –1.06 °C across the northern and southern sectors of the southern Andes, respectively (Tables VI and VII).

5.1. SPECTRAL PROPERTIES OF THE RECONSTRUCTIONS

Two spectral techniques, the Blackman-Tukey and the Multi-Tapered methods, were used to identify the most significant dominant periods in the temperature reconstructions for the northern and southern sectors of the southern Andes.

Table VI

Largest annual temperature anomalies for the northern sector (PC1) of the southern Andes

Negative		Positive	
Period	Temperature anomaly (°C)	Period	Temperature anomaly (°C)
10-year means			
1659–1668	–1.328	1924–1933	0.456
1863–1872	–0.928	1948–1957	0.387
1694–1703	–0.911	1800–1809	0.385
1850–1859	–0.867	1899–1908	0.198
1633–1642	–0.791	1935–1944	0.187
25-year means			
1647–1671	–0.952	1918–1942	0.323
1847–1871	–0.880	1944–1968	0.085
1684–1708	–0.734	1786–1810	0.033
1739–1763	–0.674		
1814–1838	–0.582		
50-year means			
1658–1707	–0.748	1915–1964	0.226
1822–1871	–0.671		
1727–1776	–0.569		

Blackman–Tukey (BTM) is the traditional method for spectral analysis (Jenkins and Watts, 1968). It is a very robust technique, unlikely to present spurious features. Its main drawback is poor resolution in the spectral domain. In our analysis, the BTM spectrum was estimated from 80 lags of autocorrelation. With this number of lags (~22% of the series length), we set a reasonable balance between high resolution and moderate stability. The number of degrees of freedom per spectral estimate is 10. The 95% confidence level of the spectrum was estimated from a 'red noise' first-order Markov null continuum based on the lag-1 autocorrelation of the time series (Mitchell et al., 1966).

The BTM spectra for the observed annual temperature variations in the northern part of the southern Andes shows that a large component of the spectral power is concentrated at cycles >10 years in length (Figure 21 left). The BTM spectrum of the past 360-year for the PC1 reconstruction also shows a large amount of spectral variance concentrated at low frequencies (Figure 21). Peaks that exceed the 95%

Table VII

Largest annual temperature anomalies for the southern sector (PC2) of the southern Andes

Negative		Positive	
Period	Temperature anomaly (°C)	Period	Temperature anomaly (°C)
10-year means			
1738–1747	–1.562	1980–1989	0.566
1658–1667	–1.534	1914–1923	0.235
1812–1821	–1.489	1960–1969	0.224
1635–1644	–1.473	1927–1936	0.015
1848–1857	–1.316		
25-year means			
1638–1662	–1.293	1968–1992	0.227
1685–1709	–1.203	1913–1937	0.053
1798–1822	–1.143		
1733–1757	–1.142		
1836–1860	–0.960		
50–year means			
1640–1689	–1.059	1944–1993	0.030
1697–1746	–1.053		
1773–1822	–0.941		
1809–1858	–0.899		
1859–1908	–0.385		

confidence limit are observed at 2.9–3.1, 3.4–3.5, 8.9–9.4, and 12.3–14.5 years. Although not statistically significant, a peak is also observed at multi-decennial scale.

We also conducted spectral analysis of the PC1 temperature reconstruction using the Multi-Taper (MTM) method (Thomson, 1990; Percival and Walden, 1993). The MTM has proven its superiority to other single-window methods of spectral analysis. It minimizes leakage outside a chosen spectral bandwidth and provides a high spectral resolution together with a signal-to-noise ratio F-test to estimate the validity of the location, amplitude and statistical significance of each peak. Statistical estimates are independent of the spectral power in the MTM method. Small amplitude oscillations may have a high significance level (Thomson, 1990). Figure 21 (left) shows the MTM spectrum for the PC1 reconstructions over the 0–0.2
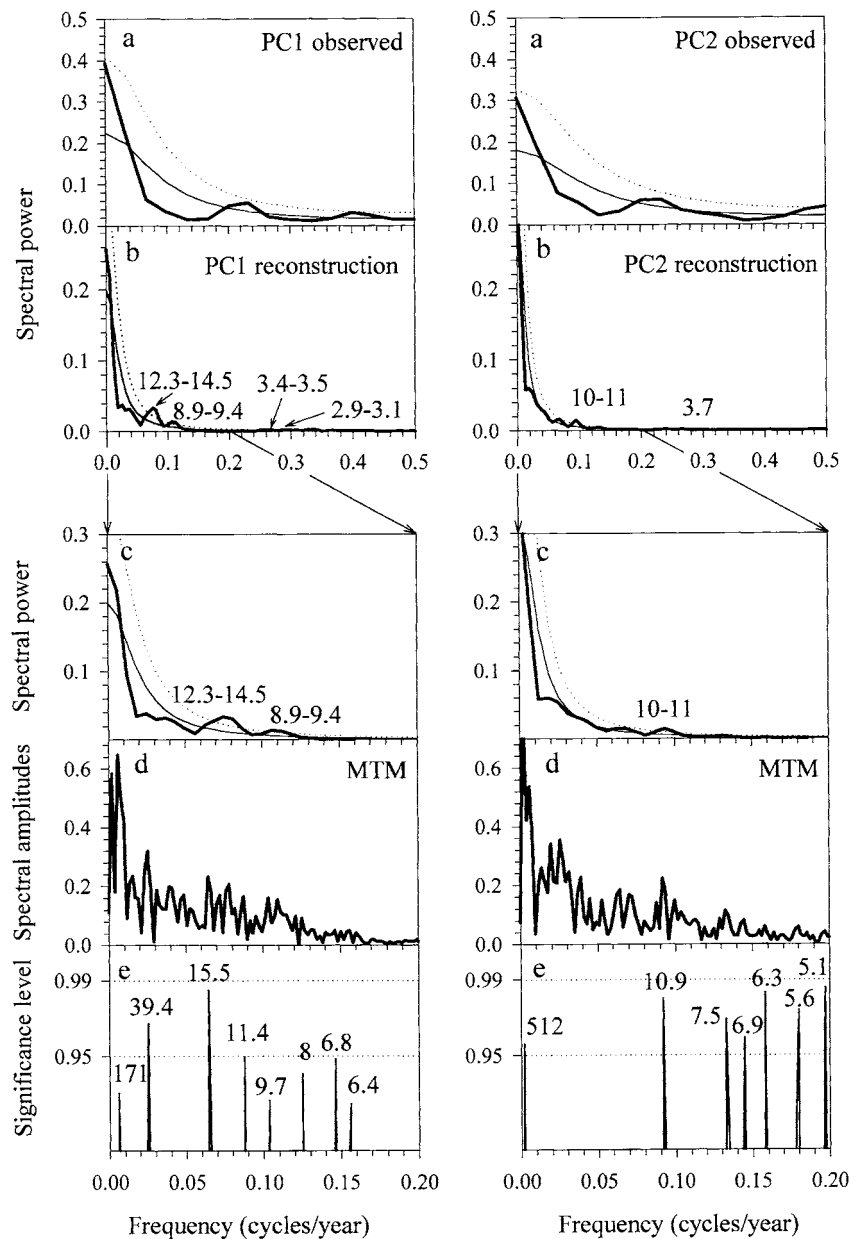
Figure 21. Blackman–Tukey (BTM) power spectra ((a), (b), and (c)) and Multi-tapered (MTM) amplitudes (d) for the temperature reconstructions in the northern (left) and southern (right) sectors of the southern Andes. The full (0–0.5 bandwidth) BTM power spectra are shown in (a) for the observed and (b) reconstructed annual temperature variations estimated over the intervals 1930–1989 and 1640–1989, respectively. An expanded view of the spectra over the 0–0.20 bandwidth is shown for the BTM in (c), the MTM amplitudes in (d) and MTM significant peaks in (e). For the BTM spectra, the 95% confidence limits (dotted lines) are based on a first-order Markov null continuum model. The vertical lines in (e) represent the amplitudes of the oscillations detected as significant above the 90% confidence level with the MTM F-test. The periods are given in years for each significant peak in the BTM and MTM spectra.

frequency range. The spectral peaks extracted using MTM are more numerous that those obtained by the BTM method. Decennial to multi-decennial spectral peaks are reported at 6.8, 11.4, 15.5 and 39.4 years (all significant at a 95% confidence MTM F-test level).

Figure 21 (right) shows the BTM spectra for the observed values of the PC2, related to the annual temperatures in the southern part of the southern Andes. Similar to the spectrum for the observed PC1 temperature pattern, a large proportion of the spectral variance is concentrated at lower frequencies. Consistent with this result, the BTM and MTM spectra for the PC2 reconstruction show marked concentrations of the spectral power at low frequencies (>30 years). A significant peak is also recorded at interannual (3.7-year) oscillations. Significant peaks (above the 95% confidence level) are observed in the MTM spectrum for oscillations centered at 5.1, 5.6, 6.3, 6.9, 7.5, 10.9 and 512 years (Figure 21, right). The soundness of the 512- year oscillation is debatable given the length of the PC2 temperature reconstruction (360 years).

Based on the comparison between the temperature reconstructions and their dominant oscillatory modes, it is clear that the two reconstructions display qualitatively similar multi-decennial and decennial scale trends. Common features in the reconstructions are the two pronounced cold intervals from 1640 to 1710 and from 1840 to 1860, the abrupt rise in temperature from 1850 to 1930, and the sustained warmth during the 20th century (Figure 20). Significant oscillations in the PC1 reconstruction at 6.4, 6.8, 8.0 and 11.4 years are coincident with cycles at 6.3, 6.9, 7.5 and 10.9 years in the PC2 reconstruction, respectively (Figure 21e, left and right). Indeed, the reconstructions are significantly correlated each other at the 99.9% confidence level accounting for the loss of degrees of freedom due to the autocorrelation in the reconstructions (Figure 22a, $r = 0.57$, $n = 360$, $N_{ef}^* = 37$). However, there are some substantial differences in the reconstructed temperature patterns. For instance, the two prominent cold events centered on 1740 and 1810 in the PC2 reconstruction are more subdued in the PC1 reconstruction. Although warmer conditions were predominant in northern Patagonia from 1780 to 1810, they were around or below the long-term mean in the south. Temperatures during the 20th century were above the long-term mean in both reconstructions, however, they showed contrasting modes of low-frequency oscillation. In coincidence with instrumental records, the reconstructions for the northern sector show that annual temperatures during the 20th century reached a peak during the 1930s and 40s, whereas in the south sector the warmest conditions were recorded during the 1980s (Figure 22a). Each reconstruction represents somewhat different spatial domains that might explain the recorded differences.

To provide a consistent measure of the coherency between the reconstructions and their most significant oscillatory modes, we calculated Pearson's correlation coefficients between the reconstructions and their long-term (decennial to centennial) oscillatory modes over 50-year common intervals lagged 10 years between periods (Figures 22b,d,f). The centennial (Figure 22c) and decennial (Figure 22e)
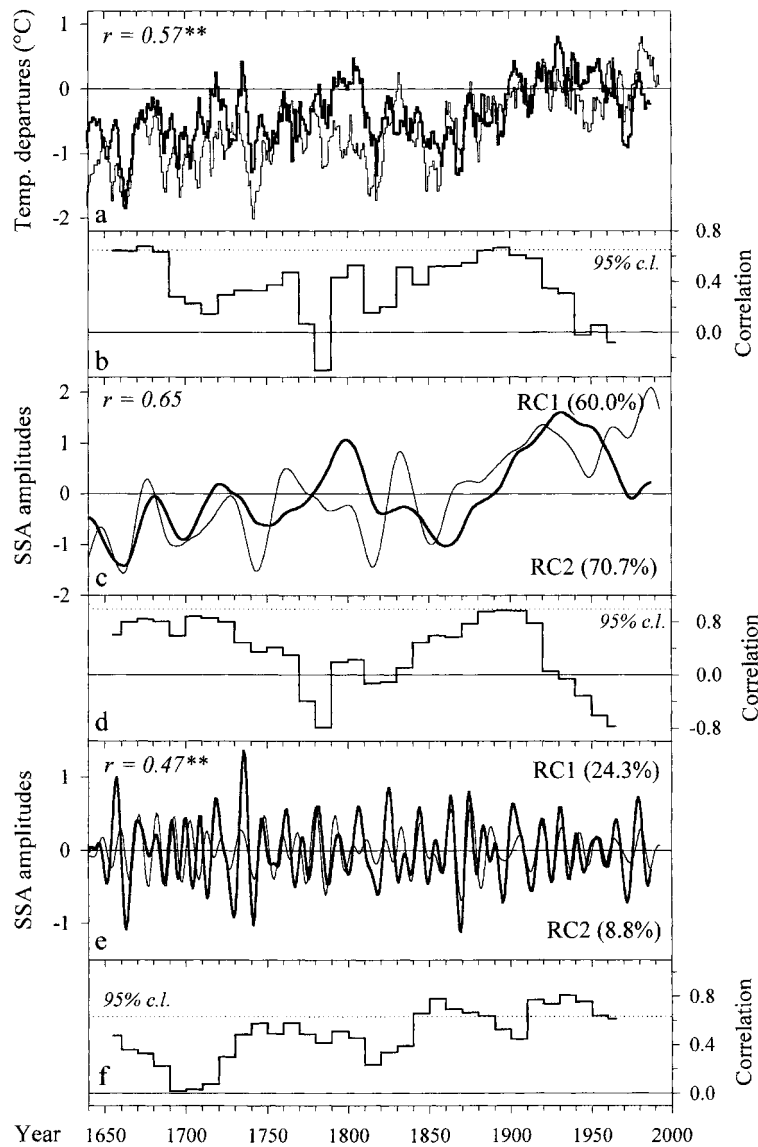
Figure 22. Comparison between the reconstructions of mean annual temperature for the northern (thick) and southern (thin) sectors of the southern Andes (a), and their most significant multi-decennial (c) and decennial (e) oscillatory modes extracted by Singular Spectrum Analysis (SSA). Moving Pearson correlation coefficients between the reconstructions and their oscillatory modes longer than 30 years, and between 11 and 29 years, are shown in (b), (d), and (f), respectively. Percentages of the original variance contributed by each of the northern and southern waveforms reconstructed by SSA are indicated in the upper and lower right corners of diagrams (c) and (e), respectively. In the upper left corners, *r* is the Pearson's correlation coefficient between the northern and southern series. Two asterisks (**) indicate correlation coefficients significant at the 99% confidence level. In (b), (d), and (e), the correlation coefficients were calculated on 50-year moving windows with an overlap of 40 years between adjacent windows, and their respective 95% confidence levels (dotted lines) adjusted for the loss of degrees of freedom due to the autocorrelation in the series.

oscillations in the reconstructions were extracted using SSA analysis (Vautard and Ghil, 1989). Barely significant positive relationships between the reconstructions occur during the cold 17th century and the transitional cold-to-warm interval from 1850 to 1930. Non-significant correlation coefficients were recorded most of the time over the past 360 years approaching to zero in the late 18th and 20th centuries (Figure 22b).

Although both secular modes show positive trends over the past 360 years, they are not significantly correlated due to the high autocorrelations in the series ($r = 0.65$, $n = 360$, $N_{ef}^* = 3$, Figure 22c). Based on 50-year windows, barely significant correlations are recorded for the centennial modes during the intervals centered at 1880, 1890 and 1900 (Figure 22d).

Most previous analyses on the Pacific SSTs have paid particular attention to the inter-decennial shift that occurred in the middle 1970s (Trenberth and Hurrell, 1984; Mantua et al., 1997; Garreaud and Battisti, 1999), a common feature in both reconstructions (Figures 22a,e). Such shifts have been occurring consistently throughout the past 400 years, with alternate regimes that last about 10–20 years at a time (Villalba et al., 2001). Pauses and accelerations in the long-term warming trends in the southern Andes may result from inter-decennial fluctuations superimposed on the centennial trends.

A comparative analysis of the inter-decennial modes of temperature fluctuations in the northern and southern sectors of the southern Andes indicates that they are significant correlated on the long-term perspective ($r = 0.47$, $n = 360$, $N_{ef}^* = 54$, Figure 22e). On the other hand, lagged correlation coefficients using the 50-year intervals for comparison reveal a contrasting pattern in the relationships between decennial modes over time (Figure 22f). Statistically significant correlations between subperiods are observed only after 1850. A major reorganization in the Pacific Ocean have been proposed at that time, which in turns may have altered the spatial patterns of the decennial oscillatory modes (Villalba et al., 2001).

The steady increase in mean annual temperatures from 1850 to 1930 is one of the most notable features in both temperature reconstructions from the southern Andes. Least-square-fitted linear trends calculated over 100-year intervals show a rate of warming close to 1.4 °C per century during the 1850–1950 interval (Figure 23). A less sustained rate of warming of 0.6 °C per century has also been recorded for the northern sector at the time of the transition from the cold interval centered on 1710 to the warm period at the beginning of the 18th century. The largest 100-year cooling trends in the northern sector of the southern Andes were centered between 1820 and 1840 in response to the temperature decline during the first half of the 19th century. No substantial cooling trends are recorded for the southern sector of the southern Andes during the past 360 years, reflecting most persistent cold conditions in higher latitudes during the interval 1640–1850.

The least-square-fitted linear trends for the PC1 and PC2 reconstructions over the interval 1856–1989 are 0.52 °C and 0.64 °C per century, as compared with 0.5 °C per century for the trend in Southern Hemisphere average land-ocean tem-
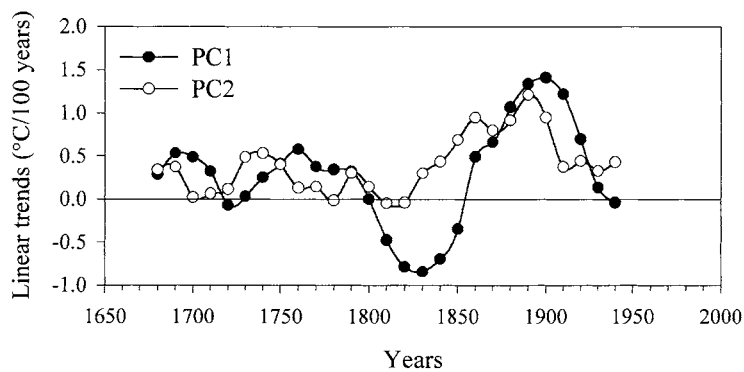
Figure 23. Linear trends over the past 360 years in the temperature reconstructions for the northern (#) and southern (∀) sectors of southern Andes estimated on 100-year moving windows with an overlap of 90 years between adjacent windows.

perature for the same period (Jones and Briffa, 1992). These small differences reflect the greater degree of increase in certain regions regarding the hemispheric means. Over the 1630–1850 period the mean trends were 0.19 °C and 0.22 °C per century, while for the whole 1630–1989 reconstructed period, the warming rates were 0.21 and 0.37 °C for the PC1 and PC2 reconstructions, respectively. Residuals about the long-term trends show significantly higher spectral energy at decennial to multi-decennial oscillations, also seen in the hemispheric instrumental data.

6. Hemispheric Links between SST and Temperature Variations

Changes in planetary circulation regimes, which in turn affect local climates, are linked to global sea surface temperature (SST) anomalies (Mo, 2000). Relationships between the dominant modes of temperature variations in southern South America and SST in the South Pacific and South Atlantic Oceans were explored to investigate how local temperature regimes are related to large-scale patterns of climate variability. Figure 24 shows contoured maps of correlation between annual SSTs with the three dominant temperature patterns derived from instrumental records shown in Figures 7–9. Correlation fields were calculated for the interval 1930–1989. SST records on a 5° latitude × 5° longitude grid were obtained from Kaplan et al. (1998). The SST dataset used here, which consists of 326 points, covers from the equator to 60° S, and from the date line (180° W) to 20° E. Coverage across the Southern Pacific and Atlantic Oceans is limited at higher latitudes. Except for the grids located along the South American coast, there is no information on SST for the southeastern Pacific south of 25° S and the South Atlantic south of 45° S. At 55° S, the SST coverage is reduced to two points off the South American coast.
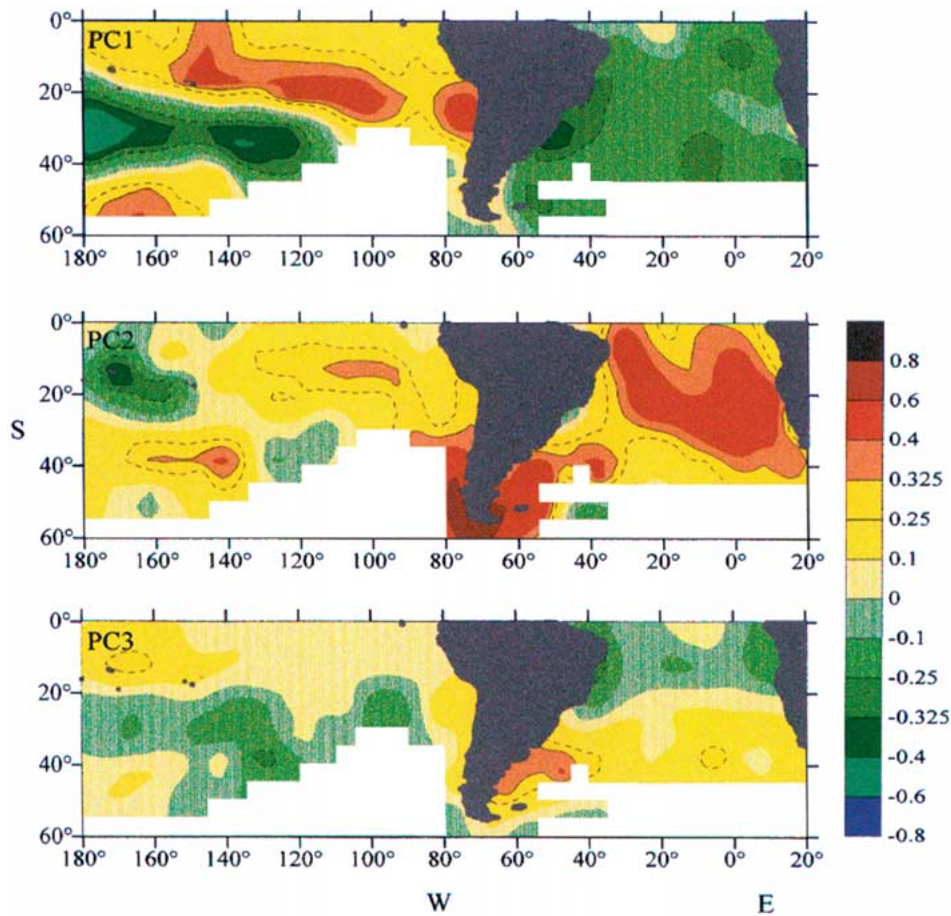
Figure 24. Spatial correlation patterns estimated during the interval 1930–1989 between annual sea-surface temperature (SST) anomalies over the South Pacific and South Atlantic Oceans and the three leading modes (Figures 7 to 9) of annual temperature variability in southern South America derived from instrumental records. Dashed and solid lines over the Oceans encircled areas significantly correlated with the temperature modes at the 95% and 99% confidence levels, respectively.

Temperature changes in the northwestern sector (PC1) of the southern Andes are closely related to central tropical-subtropical South Pacific SST oscillations (Figure 24a). Significant positive correlations in the tropical Pacific, close to the date line, penetrate eastward across the tropical-subtropical ocean reaching the Chilean coast between 20 and 40° S. In contrast, negative correlations are recorded in the extratropical western Pacific. No significant correlations are observed between PC1 and SST across the South Atlantic.

The spatial pattern that results from correlating the PC2 instrumental pattern with the South Pacific and South Atlantic SSTs is characterized by positive correlations around southern South America south of 40° S and over the tropical and
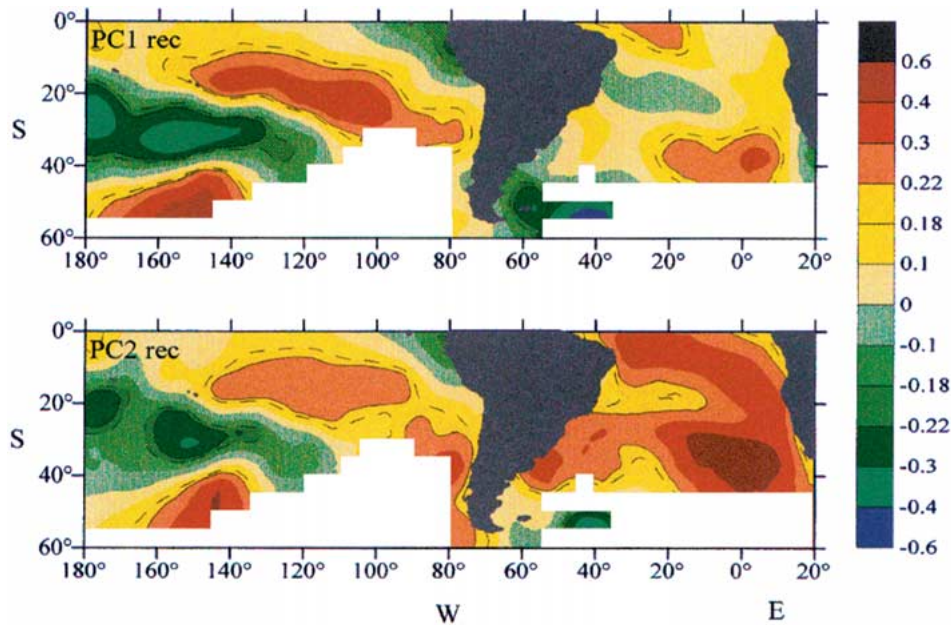
Figure 25. Spatial correlation patterns estimated during the interval 1857–1989 between annual sea-surface temperature (SST) anomalies over the South Pacific and South Atlantic Oceans and the temperatures reconstructions for the northern (PC1) and southern (PC2) sectors of the southern Andes. Note the similarity with the spatial patterns derived from instrumental records. These spatial fields resemble the 'Pacific interdecadal' and 'global warming' modes, respectively, of non-ENSO SST variability identified by Enfield and Mestas-Nuñez (2000). Dashed and solid lines over the Oceans encircled areas significantly correlated with the temperature reconstructions at the 95% and 99% confidence levels, respectively.

subtropical South Atlantic (Figure 24b). Weaker positive correlations are recorded with the subtropical Pacific centered at 100° W. In contrast to the previous spatial amplitudes, positive correlations between the temperatures on the Atlantic coast (PC3) and SSTs are much more limited and spatially reduced to a narrow belt along the Atlantic coast off southern South America from 30 to 40° S (Figure 24c).

Similar spatial patterns were obtained when the instrumental temperature (PCs) series were replaced in the calculation by the tree-ring based reconstructions, indicating that the temperature reconstructions are capturing the large-scale spatial pattern of SST (Figure 25). These maps, based on the 1857–1989 comparison interval, clearly show that the temperature reconstructions contain information about climate variability extending over much of the tropical-subtropical Pacific and over the South Atlantic to Africa. Large regions across the tropical-subtropical Atlantic have correlations above 0.3 ($n = 132$ years), and a substantial area of the subtropical Atlantic centered on 0° longitude is correlated above 0.4.

The correlation fields between the reconstructions and SST are reminiscent of some of the global modes of SST recently derived from instrumental records. The

spatial amplitudes obtained by correlating the PC1 reconstruction with the SSTs closely resemble the Southern Hemisphere counterpart of the inter-decadal mode of the Pacific SST variability identified by Garreaud and Batistti (1999), Enfield and Mestas-Nuñez (2000) and Villalba et al. (2001). In contrast to the interannual mode of El Niño/Southern Oscillation (ENSO) variability, the decadal mode is characterized by less pronounced anomalies in the eastern Pacific (the classic key ENSO region) and is not narrowly confined along the equator. In coincidence with the documented decennial oscillatory mode of Pacific SST, the spatial field of correlations between PC1 and Pacific SSTs are characterized by anomalies in the western Pacific that extent to the southeast into the subtropical South America.

In contrast to the relationships between PC1and SST, the spatial pattern that result from PC2 and SSTs across the South Pacific and South Atlantic Oceans resembles the 'global warming' mode identified by Enfield and Mestas-Nuñez (1999, 2000), and Mo (2000). According to Enfield and Mestas-Nuñez (2000), the 'global warming' mode is the ocean counterpart to the global warming seen in surface air temperatures. In agreement with our spatial pattern, the areas of significant loadings in the Southern Hemisphere for the 'global warming' mode include the east-central part of the South Pacific and the South Atlantic (Enfield and Mestas-Nuñez, 2000, their Figure 3.3b; Mo, 2000, her Figure 4a). The observed relationships between the two land-based reconstructions and SSTs over the South Pacific and South Atlantic Oceans are evidence for the existence of large-scale climate signal in the reconstructions from the southern Andes.

We follow a similar approach to Cook et al. (2000) to test the relationships between the temperature reconstructions and SST anomalies. A rotated empirical orthogonal function (EOF) analysis was carried out on the field of annual SSTs over the South Pacific and South Atlantic Ocean to establish the dominant modes of SST variability. The SST field is underdetermined for EOF analysis due to the fact that there are only 135 observations (1856–1991) for each of the 326 grid boxes. Therefore, the number of EOF to retain was determined using the Monte Carlo 'Rule-N' method (Preisendorfer et al., 1981). We found that the first ten unrotated EOFs of SST were statistically significant. These EOFs, which cumulatively explain 75% of the total variance in the SST field, were rotated using the orthogonal varimax method (Richman, 1986).

To assess which varimax factors are the most related to the temperature fluctuations in the northern and southern sectors of the southern Andes, we conducted a two-stage correlation analysis (Cook et al., 2000). First, the spatial fields shown in Figure 25 were correlated with each of the 10-correlation fields resulting from the varimax rotation. Due to the high autocorrelation in the spatial fields (nearby grids are not statistically independent), it is difficult to determine the degrees of freedom, and consequently, the significance levels for the correlations between spatial fields. On the other hand, we computed simple correlations between the temperature reconstructions and each of the ten-varimax factor scores. Those varimax factors whose spatial and score correlations with the temperature reconstructions were

nominally significant at the 95% confidence level were finally selected. Factors 6 and 8, which jointly explain 7.8% of the total variance in SSTs across the South Pacific and South Atlantic Oceans, are associated with temperature variations in the northern sector. Factors 2, 4 and 6, which collectively account for 23.6% of the variance in the SST field are the most related to temperature changes in the southern part of the southern Andes.

The varimax spatial amplitudes more closely related to PC1 and PC2 temperature reconstructions are shown in Figure 26. A visual inspection of each varimax spatial field clearly indicates where the significant correlations in Figure 25 are coming from. The spatial amplitudes in Varimax 6, which is inversely related to PC1 reconstruction, show an alternate pattern characterized by larger negative loadings in the tropical Pacific from the date line to about 120° W, a region of opposite sign in the central-subtropical Pacific, and a reduced area of negative loadings centered in the Southern Ocean at 160° W (Figure 26a). In the Varimax factor 8, positive loadings across the subtropical Pacific extend from 140° to the Chilean coast. A wedge of negative loadings starts at the date line regions and extent southward to about 120° S. Both spatial patterns show almost not connections with SSTs in the South Atlantic (Figure 26b). In consequence, the varimax rotation gives support to the influences of tropical-subtropical Pacific SST on the temperature regime in the coastal region of the northern sector (37–42° S) of the southern Andes.

Varimax factor 2, which is related to temperature variations in the southern sector, loads heavily on the SST field in the tropical Atlantic and along the western coast of Africa, whereas factor 4 represent the subtropical counterpart of factor 2 in the South Atlantic. Increased temperatures at the southern tip of South America go hand in hand with the documented increase in temperature in the South Atlantic during the 20th century (Enfield and Mestas-Nuñez, 1999, 2000). In contrast to temperature variations in the northern sector, temperatures in the southern sector of the Andes appear to be influenced by both the South Atlantic and the South Pacific Oceans. The spatial amplitude of Varimax factor 6, which is also associated with temperatures in the northern sector, is inversely correlated with the spatial pattern of correlation between PC2 and SSTs. Tropical-subtropical SSTs across the Pacific may be one of the forcing responsible for much of the commonalities seen in both temperature reconstructions.

Following Cook et al. (2000), we generated regression-weight sums of the varimax factors closely associated with the reconstructions. The best estimate of the PC1 temperature fluctuations result, not surprisingly, from adding factors 6 and 8 (Figure 27). The resulting correlation is $r = 0.58$, which suggests that one third (33.4%) of the total variance in temperature, for the northern sector of the southern Andes during the past 135 years, can be explained by a linear combination of two orthogonal modes of Pacific SST variability. On the other hand, the regression-weight sum of the factor scores 2, 4, and 6, correlates $r = 0.59$ with the PC2 reconstruction (Figure 28). The comparison between the generated
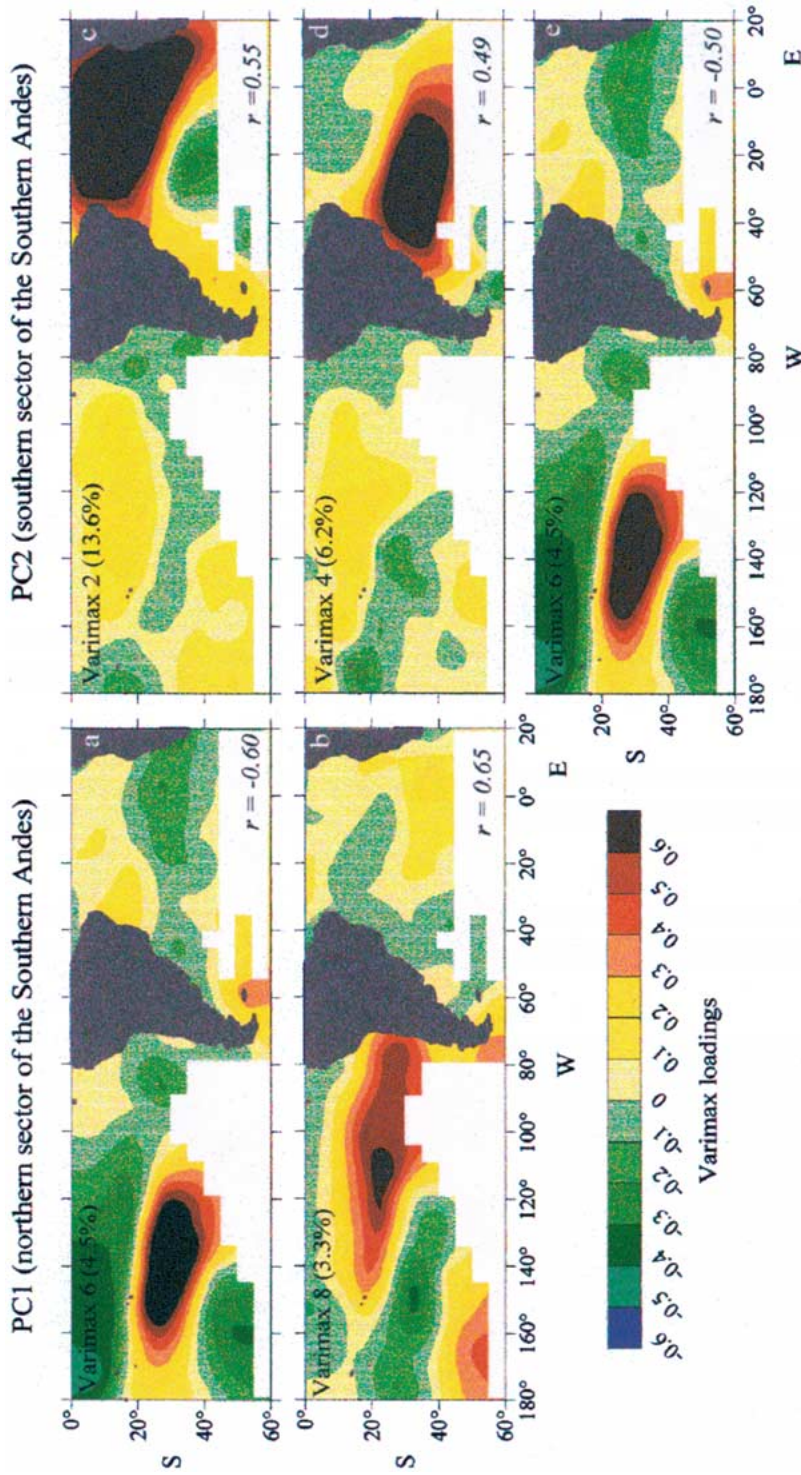
Figure 26. The four spatial fields resulting from a Varimax rotation of SST across the South Pacific and South Atlantic Oceans most highly correlated with the spatial patterns shown in Figure 25. Varimax factors 6 and 8 are the strongest correlated with the PC1 reconstruction pattern, whereas factors 2, 4, and 6 are the strongest correlated with the PC2 reconstruction pattern. The percentage of variance accounted for each factor is indicated in the upper left corners. In the lower right corners, *r* is the Pearson's correlation coefficient between the Varimax loadings and the spatial patterns in Figure 25. A comparison of these maps with those shown in Figure 25 clearly indicates where the overall patterns of correlation between the temperatures reconstructions in the southern Andes and SST anomalies are coming from.

sums and the PC2 reconstructions reveals that large part of the correlation is due to the positive secular trends in both series, whereas inter-decennial oscillations are weakly correlated (Figure 28). The lack of SST data at the southern tip of South America (only five of the 326 grids used in the varimax analysis cover the 55–60° S band) hamper any local signal to get significance in the rotated factors. The Varimax factor 6, which represents the South Pacific component in the generated sum, is the weakest correlated with PC2 ($r = 0.20$). However, it inclusion in the final regression-weighted sum improves the correlation with PC2 ($r = 0.59$). In summary, annual air temperatures across the southern Andes are clearly related to large-scale anomalies in SSTs, particularly those in the tropical-subtropical Pacific and Atlantic Oceans. Four discrete modes (factors 2 and 4 over the Atlantic, factors 6 and 8 over the Pacific) are largely responsible for the observed relationships.

7. Discussion and Conclusions

In the current debate on the magnitude of the 20th century climatic changes, there is a growing appreciation of the importance of high-resolution records from the past. By studying the records of past climate variability it is possible to establish how the climate systems varied under natural conditions, before the human-induced changes in the atmosphere became significant. Tree-rings, which provide continuous records with annual to seasonal resolution, are a source of information on the past natural climatic variability and allow us to set the most recent climate changes in the context of the past few centuries to millennia. In this paper, we combined instrumental records from southern South America, SST across the South Pacific and South Atlantic Oceans, and tree-ring chronologies to provide the most consistent view of temperatures variations in the southern Andes during the past 360 years and their relationships with internal climatic forcings.

Based on instrumental records, regional analysis of mean annual temperature changes have been presented for southern Chile and Argentina by Rosenblüth et al. (1995, 1997) and for decadal means for Argentinean stations by Hoffman (1990). Temperature trends were discussed in these studies based on single station records. Building on these studies, we determined the dominant temperature regimes in southern South America during the 20th century and their geographical representativeness. Three different spatial temperature patterns can be recognized in southern South America during the 20th century: (1) Surface cooling from 1930 to 1990 on the station located on northern sector of the southern Andes by the Pacific Coast (37–42° S), (2) No significant changes in surface temperature on the stations located by the Atlantic Ocean north of 45° S, and (3) A remarkable surface warming from 46 to 55° S (Figures 6–9).

The cooling period in mid-latitudes from the 1950s and 1960s as shown by Temuco, Valdivia and Puerto Montt stations (Figure 7), is not presented at the radiosonde observations at these locations at 700 hPa and above (Aceituno et al.,
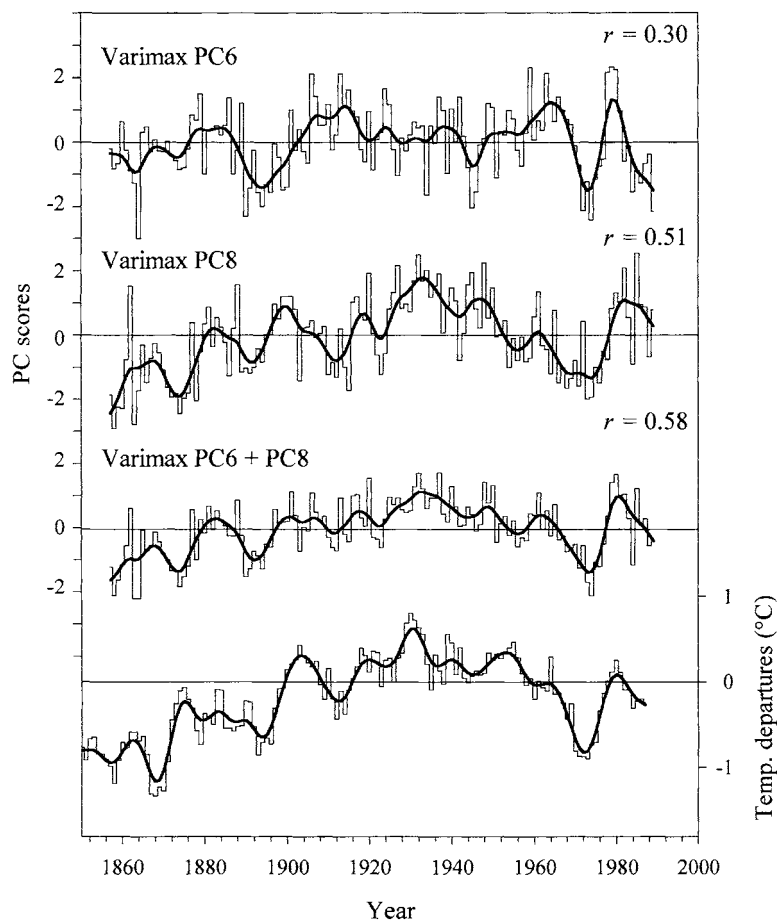
Figure 27. Regression-weighted sums of the Varimax factor scores 6 and 8 significantly correlated (at the 95% confidence level) with the temperature reconstruction for the northern sector of the southern Andes. The Pearson's correlation coefficients (r) between the Varimax factor scores, its respective regression-weighted sum, and the reconstruction of annual temperature for the northern sector of the southern Andes, during the interval 1857–1989, are indicated.

1993). This cooling on the continent seems to be a local feature of the South America mid-latitudes, mostly on the Pacific side. The Argentinean stations located at the same latitude on the eastern slope of the Andes exhibit a positive trend due to a temporary recovery in recent years (see Figure 4). The remarkable warming at southern latitudes is in agreement with the large temperature increase reported by King (1994) for the Antarctic Peninsula.

When seasonal temperature means are compared, it becomes apparent that both warming or cooling trends are more intense in summer (December to February), a contrasting feature with temperature trends at higher latitudes in the Northern Hemisphere. Because the mature phase of El Niño events normally occurs during
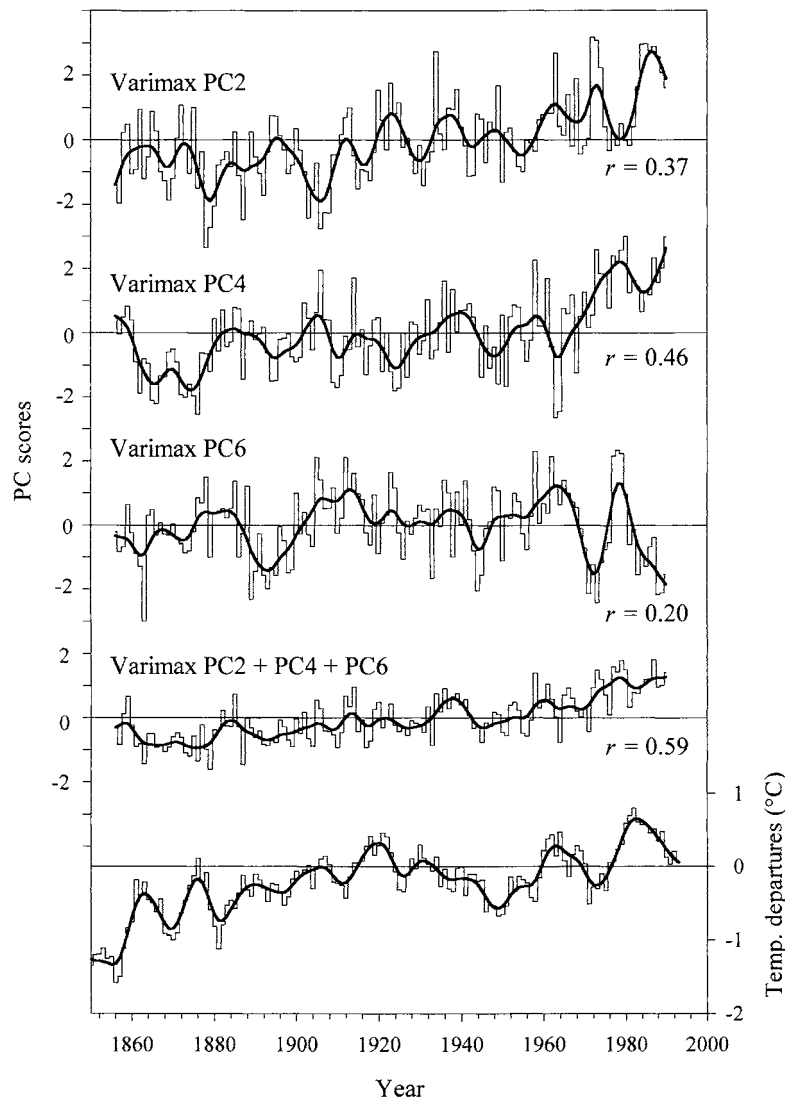
Figure 28. Regression-weighted sums of the Varimax factor scores 2, 4 and 6, which are significantly correlated (at the 95% confidence level) with the temperature reconstruction for the southern sector of the southern Andes. The Pearson's correlation coefficients (*r*) between the Varimax factor scores, its respective regression-weighted sum, and the reconstruction of annual temperature for the southern sector of the southern Andes, during the interval 1857–1989, are indicated.

the austral summers, ENSO phenomena might be partially responsible for this contrast between seasonal temperature changes at higher latitudes in both hemispheres. On the other hand, both positive and negative trends in southern South America are due mostly to changes in minimum temperatures (Rosenblüth et al., 1997), a feature commonly observed in other regions of the world (Karl et al., 1993).

In the Southern Hemisphere, the surface temperature changes after 1976 were noticed as a cooling in the central subtropical Pacific and as a warming over the central tropical and eastern subtropical Pacific (Graham, 1994). Van Loon et al. (1993) noted a sudden change in the Southern Hemisphere circulation after 1976. The zonal wave 3 intensified in midlatitudes, while sea level pressure fell over Antarctica. After these abrupt changes in the circulation regime in 1976, minimum temperatures along the Chilean coast warm up significantly (Rosenblüth et al., 1997). For most stations in southern South America, the increase in annual temperature after 1976 is dominated by the summer warming. Indeed, the summer conditions are largely responsible for the positive trends in annual temperature observed in the stations located on the eastern slope of the Andes in northern Patagonia and at higher latitudes (Figures 4 and 5). These temperature changes are compatible with the teleconnection patterns described by Karoly (1989) for the Southern Hemisphere during the El Niño years. The 1976 shift appears as more 'El Niño-like' conditions in the equatorial Pacific. Unlike classic El Niño anomalies, SST anomalies associated with this decennial mode reach into mid-latitudes of both hemispheres. For the extratropical South Hemisphere, the most relevant anomaly associated with this pattern is an anticyclonic circulation extending from the date line to the southern tip of South America (Garreaud and Battisti, 1999). The midlatitude westerly winds across the region are weakened in response to this anticyclonic anomaly. In addition, the NCEP-NCAR reanalysis data indicate that wintertime low-level air temperature over the Southern Oceans since 1977 has been nearly 2 °C warmer than the mean from the interval 1958–1976 (Garreaud and Battisti, 1999). SSA analysis from our reconstructions (Figure 21) indicates that the inter-decennial mode has persisted for at least during the past 400 years. Periods of low energy (or reduced amplitudes) such as the interval 1930–1970 are recognized in the inter-decennial mode (Figure 21e). Consistent with our observations, it has been indicated that the ENSO phenomenon has fluctuated between more robust periods from the 1870s to 1910s and during the 1970s–80s, a less energetic or quiescent from the 1920s to the 1960s (Allan, 2000). The abrupt change toward warmer SSTs at 1976 is the most obvious feature of the decennial-scale oscillatory mode over the Pacific during the past 130 years (Villalba et al., 2001). Interestingly, the growth of *Nothofagus pumilio* at upper treeline has been anomalously high since 1977 at most temperature-sensitive sites in the southern Andes (Villalba et al., 1997).

These new temperature reconstructions represent a significant improvement over previous reconstructions in southern South America in terms of spatial representativeness, sample replication, and statistical fidelity of the reconstructed oscillations from inter-decennial to centennial time scales. Millenium-long temperature reconstructions have been previously developed from *Fitzroya cupressoides* for northern Patagonia (Villalba, 1990; Lara and Villalba, 1993), but they have been based on single chronologies and the application of standardization methods with limited capacity to recover the low-frequency oscillations in the tree-ring series.

The new reconstructions, which have been modeled to emphasize inter-centennial differences in temperature, reveal how unusual climate conditions during the 20th century have been in the context of the past 400 years. Warmer conditions during the 1930s and 1940s across the northern sector of the southern Andes were unprecedented in the 360-year reconstruction (Figure 20). Similarly, temperatures in the southern sector since mid-1970 have reached unparalleled levels in the past 360 years (Figure 20). In both records, long-lasting cold periods are observed from 1640 to 1670, and during the mid-19th century. The reconstructions thus describe a well-defined cold interval from ∼1640–1850, which conforms with the consensus view of the 'Little Ice Age', a term commonly used to describe these cold episodes on global scale (Bradley and Jones, 1993). Although this period was not uniformly cold and temperature anomalies differed regionally (Figure 21), overall it was significantly below the 1900–1990 means by as much as 0.53 °C and 0.86 °C in the northern and southern sectors respectively. Consequently, the temperature variations instrumentally recorded during the 20th century document a narrow window of a climatic event that began in the mid-19th century and marked the end of the 'Little Ice Age' in the southern Andes.

Supporting evidences for the reliability of our temperature estimates comes from comparison with glacier records. The glacier record provides estimates of overall temperature changes from one century to the next (Luckman and Villalba, 2001). Generalized glacier retreat has been observed in the 20th century across the southern Andes in response to the documented climatic changes. Treeless glacier deposits around most Patagonian glaciers are evidence of glacier retreat since the late Neoglacial advance (Villalba, 1994; Luckman and Villalba, 2000). The reduction of ice masses accumulated over preceding centuries has continued (or accelerated) to the present. Indeed, all land based glaciers and most calving glaciers in the Northern and Southern Patagonian Icefields are presently retreating and thinning at fast rate (Naruse and Aniya, 1992; Casassa, 1995). From the reconstructed temperature records it is suggested that the generalized glacier retreat is largely due to the temperature increase during the 20th century in both northern and southern latitudes of the southern Andes. However, the glacier retreat must also be affected by the regional decrease in precipitation along the Pacific coast in southern South America (Rosemblüth et al., 1995).

There are interesting similarities between our reconstructions from the southern Andes and some temperature reconstructions from the higher latitudes of the Northern Hemisphere. A compilation of paleoclimate records from lake sediments, trees, glaciers, and marine sediments was conducted by Overpeck et al. (1997) to provide a view of Circum-Arctic climatic variability over the past 400 years. The most notable feature of temperature change revealed by most records across the Arctic is the ubiquitous transition from anomalous cold conditions in the mid-19th century to anomalous warm in the mid-20th century. Similar to our reconstructions for higher latitudes in the Southern Hemisphere, the rate of temperature increase from 1850 to 1920 was the highest over the past 400 years (Overpeck et al., 1997).

It appears that the 19th to 20th-century warming was 1 to 3 °C locally (Jacoby and D'Arrigo, 1992; Jones and Bradley, 1993; Briffa et al., 1996) and averaged about 1.5 °C across the Arctic, as compared to warmings of 1.62 °C (1848–1930) and 2.04 °C (1849–1921) for the northern and southern areas of the southern Andes, respectively. In contrast, on both global and hemispheric means the temperature trends from the late 1850s to the 1910s are almost flat (WMO, 1998), suggesting that high latitudes in both hemispheres share common features in temperature changes, which are not present on global scales.

The potential for the low-frequency changes in SST to influence climate on the continents can be seen in many analyses of the joint variability of anomalies in SST, tropospheric pressure and wind fields (Trenberth and Hurrell, 1994; Gareaud and Battisti, 1999; Allan, 2000). Enfield and Mestas-Nuñez (2000) have suggested that the oceans play the role of pacemaker, introducing persistence into the troposphere, which in turn can condition long-term variations in climate. Indeed, in a recent paper by Mo (2000), who examined the long-term trends of large-scale circulation regimes in the Southern Hemisphere using the NCEP-NCAR reanalysis, it is clearly shown that the leading modes of atmospheric circulation are connected to global changes in SSTs. In the low-frequency band, the leading mode of circulation regime in the Southern Hemisphere shows a strong zonal symmetry with a phase reversal between high- and mid-latitudes. A wavenumber 3, associated with this mode, has its centers of action located on the three southern oceans. This mode is related to SST anomalies with positive loadings over the three southern oceans and negative loadings in the western North Pacific and the North Atlantic (Mo, 2000, her Figure 3c, which is also coincident with the 'global warming' mode of Enfield and Mestas-Nuñez, 2000). The temporal evolution (PC scores) of this leading mode is linked to the documented warming of the southern oceans. Its atmospheric counterpart is characterized by the falling of sea level pressure over Antarctica and the rising over areas near New Zealand and South America (Van Loon et al., 1993; Mo, 2000). The 20th century increase in temperature documented in this paper for the southern Andes is the local atmospheric response to these large-scale, ocean-atmosphere changes. Indeed, the northerly flow of air masses across the region, measured as the sea level pressure differences between Punta Arenas (53°00', 70°51') and Stanley (51°29' S, 57°36' W), has markedly increased during the 20th century in comparison to the 19th century (Villalba et al., submitted).

The second and third modes of low-frequency variability in the Southern Hemisphere are the Pacific-South American (PSA) patterns (Mo, 2000). They are characterized by a wavenumber 3 in quadrature with each other and a well-defined wave train from tropical Pacific to southern South America. The larger amplitudes of these modes are in the Pacific-South America sector. The PSA mode, associated with enhanced convection in the tropical central Pacific is the major atmospheric response to El Niño-Southern Oscillation (ENSO) in the Southern Hemisphere (Karoly, 1989). The sudden change of climate regimes around 1976 is present in the temporal evolution of PSA circulation modes. The spatial correlation

field between the PSA modes and SST resemble the PDO patterns, with positive loadings extending from the central-eastern Pacific to the extratropical coasts of North and South America. Negative SST anomalies occur over the western North and South Pacific. A similar spatial pattern is observed when our reconstruction of annual temperatures for the northern sector of the southern Andes is regressed against the South Pacific SSTs. On decennial timescales, temperature changes in the central and eastern Pacific are linked to the strength of the PSA mode (Mo, 2000). In contrast to the southern sector, these findings suggest that temperature variations in the northern sector of the southern Andes are closer related to the 'Pacific inter-decennial' instead of the 'global warming' mode.

Acknowledgements

References

Aceituno, P., Fuenzalida, H., and Rosenblüth, B.: 1993, 'Climate along the Extratropical Coast of South America', in Mooney, H. A., Fuentes, E. R., and Kronberg, B. I. (eds.), *Earth Systems Responses to Global Change: Contrast between North and South America*, Academic Press, New York, U.S.A., pp. 61–69.

Alexandersson, H.: 1986, 'A Homogeneity Test Applied to Precipitation Data', *J. Climatol.* **6**, 661–675.

Allan, R. J.: 2000, 'ENSO and Climatic Variability in the Past 150 Years', in Diaz, H. and Markgraf, V. (eds.), *El Niño and the Southern Oscillation, Multiscale Variability and Global and Regional Impacts*, Cambridge University Press, pp. 3–56.

Almeyda, A. E. and Saez. S. F.: 1958, *Recopilación de datos climáticos de Chile y mapas sinópticos respectivos*, Ministerio de Agricultura, Santiago, Chile.

Aravena, J. C., Lara, A., Wolodarsky, A., and Cuq, E.: 2000, 'Dendroclimatology of *Nothofagus pumilio* Forests in the Upper Treeline of Magallanes Region, Chile', *International Conference on Dendrochronology for the Third Millenium*, Abstracts Vol., Mendoza, Argentina, 216 pp.

Beniston, M. (ed.): 1994, *Mountain Environments in Changing Climates*, Routledge Publishing Co., London and New York, 492 pp.

Blasing, T. J., Solomon, A. M., and Duvick, D. N.: 1984, 'Response Functions Revisited', *Tree-Ring Bull.* **44**, 1–15.

Boninsegna, J. A., Keegan, J., Jacoby, G. C., D'Arrigo, R. D., and Holmes, R. L.: 1989, 'Dendrochronological Studies in Tierra del Fuego, Argentina', *Quaternary of South America and Antarctic Peninsula* **7**, 315–326.

Bradley, R. S.: 1999, 'Paleoclimatology: Reconstructing Climates of the Quaternary', Academic Press, San Diego, U.S.A., 610 pp.

Bradley, R. S. and Jones, P. D.: 1993, 'Little Ice Age Summer Temperature Variations: Their Nature and Relevance to Recent Global Warming Trends', *The Holocene* **3**, 367–376.

Bretherton, C. S., Widmann, M., Dymnikov, V. P., Wallace, J. M., and Blade, I.: 1999, 'The Effective Number of Spatial Degrees of Freedom of a Time-Varying Field', *J. Climate* **12**, 1990–2009.

Briffa, K. R.: 1995, 'Interpreting High-Resolution Proxy Climate Data – The Example of Dendroclimatology', in von Storch, H. and Navarra, A. (eds.), *Analysis of Climate Variability, Applications of Statistical Techniques*, Springer, Berlin, pp. 77–94.

Briffa, K. R., Jones, P. D., Bartholin, T. S., Eckstein, D., Schweingruber, F. H., Karlen, W., Zetterberg, P., and Eronen, M.: 1992, 'Fennoscandian Summers from AD 500: Temperature Changes on Short and Long Time Scales', *Clim. Dyn.* **7**, 111–119.

Briffa, K. R., Jones, P. D., Bartholin, T. S., Schweingruber, F. H., Karlen, W., and Shiyatov, S. G.: 1996, 'Tree-Ring Variables as Proxy-Climate Indicators: Problems with Low-Frequency Signals', in Jones, P. D., Bradley, R. S., Jouzel, J. (eds), *Climate Variations and Forcing Mechanisms of the Last 2000 Years*, NATO ASI Series, Vol. I41, Springer, Heidelberg, pp. 9–41.

Casassa, G.: 1995, 'Glacier Inventory in Chile: Current Status and Recent Glacier Variations', *Ann. Glaciol.* **21**, 317–322.

Cook, E. R.: 1987, 'The Decomposition of Tree Ring Series for Environmental Studies', *Tree-Ring Bull.* **47**, 37–59.

Cook, E. R., Briffa, K., Shiyatov, S., and Mazepa, V.: 1990, 'Tree-Ring Standardization and Growth-Trend Estimation', in Cook, E. and Kairiukstis, L. (eds.), *Methods of Dendrochronology*, Kluwer Academic Publishers, Amsterdam, The Netherlands, pp. 104–132.

Cook, E. R., Buckley, B. M., D'Arrigo, R. D., and Peterson, M. J.: 2000, 'Warm-Season Temperatures since 1600 BC Reconstructed from Tasmanian Tree Rings and their Relationship to Large-Scale Sea Surface Temperature Anomalies', *Clim. Dyn.* **16**, 79–91.

Cook, E. R. and Peters, K.: 1981, 'The Smoothing Spline: A New Approach to Standardizing Forest Interior Ring-Width Series for Dendroclimatic Studies', *Tree-Ring Bull.* **41**, 45–53.

Cooley, W. W. and Lohnes, P. R.: 1971, *Multivariate Data Analysis*, Wiley, New York, U.S.A.

De Fina, A. L.: 1972, 'El clima de la región del los bosques andino-patagónicos argentinos', in Dimitri, M. J. (ed.), *La región de los bosques andino-patagónicos*, Colección Científica del INTA, **10**, 35–58.

Diaz, H. F. and Kiladis, G. N.: 1992, 'Atmospheric Teleconnections Associated with the Extreme Phases of the Southern Oscillation', in Diaz, H. F. and Markgraf, V. (eds.), *El Niño: Historical and Paleoclimatic Aspects of the Southern Oscillation*, Cambridge: Cambridge University Press, pp. 7–28.

Doake, C. S. M. and Vaughan, D. G.: 1991, 'Rapid Disintegration of the Wordie Ice Shelf in Response to Atmospheric Warming', *Nature* **350**, 328–330.

Draper, N. R. and Smith, H.: 1981, *Applied Regression Analysis*, 2nd edn., John Wiley and Sons, New York, U.S.A.

Ebbesmeyer, C. C., Cayan, D. R., McLain, D. R., Nichols, F. H., Peterson, D. H., and Redmond, K. T.: 1991, '1976 Step in the Pacific Climate: Forty Environmental Changes between 1968–75 and 1977–84', in Betancourt, J. L. and Tharp, V. L. (eds.), *Proceedings of the 7th Annual Pacific Climate Workshop*, California Department of Water Resources, Interagency Ecological Studies Program, Report 26, pp. 115–126.

Enfield, D. B. and Mestas-Nuñez, A. M.: 1999, 'Multiscale Variabilities in Global Sea Surface Temperature and their Relationships with Tropospheric Climate Patterns', *J. Climate* **12**, 2719–2733.

Enfield, D. B. and Mestas-Nuñez, A. M.: 2000, 'Global Modes of ENSO and Non-ENSO Sea Surface Temperature Variability and their Associations with Climate, in Diaz, H. and Markgraf, V. (eds.),

El Niño and the Southern Oscillation, Multiscale Variability and Global and Regional Impacts, Cambridge University Press, pp. 89–112.

Fritts, H. C.: 1976, *Tree Rings and Climate*, Academic Press, London.

Gallopín, G. C.: 1978, 'Estudio ecológico integrado de la cuenca superior del Río Manso Superior (Río Negro, Argentina). I. Descripción general de la cuenca', *Anales de Parques Nacionales* **14**, 161–230.

Garreaud, R. and Battisti, D. S.: 1999, 'Interannual and Interdecadal (ENSO-Like) Variability in the Southern Hemisphere Tropospheric Circulation', *J. Climate* **12**, 2113–2123.

Geiger, R.: 1965, *The Climate near the Ground*, Harvard University Press, Cambridge, Massa-chusetts, U.S.A., 277 pp.

Graham, N. E.: 1994, 'Decadal-Scale Climate Variability in the 1970s and 1980s: Observations and Model Results', *Clim. Dyn.* **10**, 135–162.

Guiot, J.: 1990: 'Methods of Calibration', in Cook, E. R. and Kairiukstis, L. A. (eds.), *Methods of Dendrochronology. Applications in the Environmental Sciences*, Kluwer Academic Publishers, Dordrecht, pp. 165–178.

Gordon, G. A. and LeDuc, S. K.: 1981, 'Verification Statistics for Regression Models', in Am. Meteorol. Soc. (ed.), *Preprints Seventh Conference on Probability and Statistics in Atmospheric Sciences*, Monterey, California, U.S.A., pp. 129–133

Hoffman, A. J.: 1990, 'De las variaciones de la temperatura del aire en la Argentina y estaciones de la zona subantártica adyacente, desde 1903 hasta 1989 inclusive', *Primera Conferencia Lati-noamericana sobre Geofísica, Geodesia e Investigación Espacial Antárcticas*, Buenos Aires, pp. 160–168.

Jacoby, G. C. and D'Arrigo, R. D.: 1989, 'Reconstructed Northern Hemisphere Annual Temperature since 1671 Based on High-Latitude Tree-Ring Data from North America', *Clim. Change* **14**, 39–49.

Jenkins, G. M. and Watts, D. G.: 1968, *Spectral analysis and its applications*, Holden-Day, San Francisco, U.S.A., 525 pp.

Jobbágy, E. G., Paruelo, J. M., and León, R. J. C.: 1995, 'Estimación del régimen de precipitación a partir de la distancia a la cordillera en el noroeste de la Patagonia', *Ecología Austral* **5**, 47–54.

Jones, P. D. and Briffa, K. R.: 1992, 'Global Surface Air Temperature Variations during the Twentieth Century: Part 1, Spatial, Temporal and Seasonal Details', *The Holocene* **2**, 165–179.

Kaplan, A., Cane, M. A., Kushnir, Y., Clement, A. C., Blumenthal, M. B., and Rajagopalan, B.: 1998, 'Analyses of Global Sea Surface Temperature 1856–1991', *J. Geophys. Res.* **103**, 1856–18589.

Karl, T. R., Jones, P. D., Knight, R. W., Kukla, G., Plummer, N., Gallo, K. P., Lindesay, J., Charl-son, R. J., and Peterson, T. C.: 1993, 'Asymmetric Trends of Daily Maximum and Minimum Temperature', *Bull. Amer. Meteorol.* **74**, 1007–1023.

Karoly, D. J.: 1989, 'Southern Hemisphere Circulation Features Associated with El Niño-Southern Oscillation', *J. Climate* **2**, 1239–1252.

King, J. C.: 1994, 'Recent Climate Variability in the Vicinity of the Antarctic Peninsula', *Int. J. Clim.* **14**, 357–369.

Köner, C.: 1999, *Alpine Plant Life. Functional Plant Ecology of High Mountain Ecosystems*, Springer, Berlin.

Lara, A., Aravena, J. C., Villalba, R., Wolodarsky-Franke, A., Luckman, B. H., and Wilson, R.: 2001, 'Dendroclimatology of High-Elevation *Nothofagus pumilio* Forests at their Northern Distribution Limit in the Central Andes of Chile, *Can. J. Forest Res.* **31**, 925–936.

Lara, A. and Villalba, R.: 1993, 'A 3620-Year Temperature Record from *Fitzroya cupressoides* Tree Rings in Southern South America', *Science* **260**: 1104–1106.

Luckman, B. H. and Boninsegna, J. A.: 2001, 'The Assessment of Present, Past and Future Climate Variability in the Americas from Treeline Environments', *PAGES News* **9**, 17–19.

Luckman, B. H. and Villalba, R.: 2001, 'Assessing the Synchroneity of Glacier Fluctuations in the Western Cordillera of the Americas during the Last Millennium', in Markgraf, V. (ed.), *Inter-Hemispheric Climate Linkages*, Academic Press, San Diego, Califormia, U.S.A., pp. 119–140.

Mantua, J. N., Hare, S. R., Zhang, Y., Wallace, J. M., and Francis, R. C.: 1997, 'A Pacific Interdecadal Climate Oscillation with Impacts on Salmon Production', *Bull. Amer. Meteorol.* **78**, 1069–1080.

Masiokas, M. H., Villalba, R., Trombotto, D., Delgado,S., Luckman, B., Ripalta, A., and Hernandez, J.: 2001, 'Dendrogeomorphological Reconstruction of Glacier Variations in Northern Patagonia during the Past 1000 Years', in Kaennel Dobbertin, M. and Bräker, O. U. (eds.), *International Conference on Tree Rings and People*, Abstracts, Swiss Federal Research Institute WSL, Birmensdorf, Switzerland.

Miller, A.: 1976, 'The Climate of Chile', in Schwerdtfeger, W. (ed.), *World Survey of Climatology. Climates of Central and South America*, Elsevier, Amsterdam, The Netherlands, pp. 113–131.

Mitchell, J. M. Jr., Dzerdseevskii, B., Flohn, H., Hofmeyr, W. L., Lamb, H. H., Rao, K. N., and Wallen, C. C.: 1966, *Climatic Change, World Meteorological Organization*, Technical Note 79, pp. 79.

Mo, K.: 2000, 'Relationships between Low-Frequency Variability in the Southern Hemisphere and Sea Surface Temperature Anomalies', *J. Climate* **13**, 3599–3610.

Naruse, R. and Aniya, M.: 1992, 'Outline of Glacier Research Project in Patagonia', *Bull. Glacier Res.* **10**, 31–38.

Osborn, T. J., Briffa, K. R., and Jones, P. D.: 1997, 'Adjusting Variance for Sample-Size in Tree-Ring Chronologies and other Regional-Mean Time Series', *Dendrochronologia* **15**, 89–99.

Overpeck, J., Hughen, K., Hardy, D., Bradley, R., Case, R., Douglas, M., Finney, B., Gajewski, K., Jacoby, G., Jennings, A., Lamoureux, S., Lasca, A., MacDonald, G., Moore, J., Retelle, M., Smith, S., Wolfe, A., and Zielinski, G.: 1997, 'Arctic Environmental Change of the Last Four Centuries', *Science* **278**, 1251–1256.

Percival, D. B. and Walden, A. T.: 1993, 'Multitaper Spectral Estimation', in Percival D. B. and Walden A. T. (eds.), *Spectral Analysis for Physical Applications: Multitaper and Conventional Univariate Techniques*, Cambridge University Press, Cambridge, pp. 331–337.

Preisendorfer, R. W., Zwiers, F. W., and Barnett, T. P.: 1981, *Foundations of Principal Components Selection Rules*, SIO Ref. Ser. 81-14, Scripps Institution of Oceanography, La Jolla, California, U.S.A.

Prohaska, F.: 1976, 'The Climate of Argentina, Paraguay and Uruguay', in Schwerdtfeger, W. (ed.), *World Survey of Climatology, Climates of Central and South America*, Elsevier, Amsterdam, The Netherlands, pp. 13–112.

Priestley, M. B.: 1992, *Spectral Analysis and Time Series*, Academic Press, London.

Quinn, W. H.: 1992, 'A Study of Southen Oscillation-Related Climatic Activity for A.D. 622–1990 Incorporating Nile River Flow Data', in Diaz, H. F. and Markgraf, V. (eds.), *El Niño: Historical and Paleoclimatic Aspects of the Southern Oscillation*, Cambridge University Press, Cambridge, pp. 119–149.

Richman, M. B.: 1986, 'Rotation of Principal Components: A review', *J. Climatol.* **6**, 293–336.

Roig, F. A., Aravena, J. C., and Lara, A.: 2000, 'Tree-Ring Studies from Upper Treeline Environments of Tierra del Fuego and Navarino Island', *International Conference on Dendrochronology for the Third Millenium*, Abstracts Vol., Mendoza, Argentina, 239 pp.

Rosenblüth, B., Casassa, G., and Fuenzalida, H.: 1995, 'Recent Climatic Changes in Western Patagonia', *Bull. Glacier Res.* **13**, 127–132.

Rosenbluth, B., Fuenzalida, H. A., and Aceituno, P.: 1997, 'Recent Temperature Variations in Southern South America', *Int. J. Clim.* **17**, 67–85.

Taljaard, J. J.: 1972, 'Synoptic Meteorology of the Southern Hemisphere', *Meteorological Monographs* **13**, 139–213.

Thomson, D. J.: 1990, 'Time Series Analysis of Holocene Climate Data', *Phil. Trans. Roy. Soc. London* **330**, 601–616.

Tranquillini, W.: 1979, *Physiological Ecology of the Alpine Timberline*, Springer-Verlag, New York, U.S.A., 137 pp.

Trenberth, K. E.: 1990, 'Recent Observed Interdecadal Climate Changes in the Northern Hemisphere', *Bull. Amer. Meteorol.* **71**, 988–993.

Trenberth, K. E. and Hurrell, J. W.: 1994, 'Decadal Atmosphere-Ocean Variations in the Pacific', *Clim. Dyn.* **9**, 303–319.

Schmelter, A.: 2000. *Climatic Response and Growth-Trends of* Nothofagus pumilio *along Altitudinal Gradients from Arid to Humid Sites in Northern Patagonia*, Ph.D. Dissertation, Universität Bonn, Bonn, Germany.

Schwerdtfeger, W.: 1960, 'The Seasonal Variation of the Strength of the Southern Circulation Vortex', *Mon. Wea Rev.* **88**, 203–208.

Schwerdtfeger, W.: 1962, *Meteorología del área del Pasaje de Drake', Servicio de Hidrografía Naval*, Secretaría de Marina, Buenos Aires, 78 pp.

Van Loon, H., Kidson, J. W., and Mullan, A. N.: 1993, 'Decadal Variation of the Annual Cycle in the Australian Dataset', *J. Climate* **6**, 1227–1231.

Vautard, R. and Ghil, M.: 1989, 'Singular Spectrum Analysis in Nonlinear Dynamics, with Applications to Paleoclimatic Time Series', *Physica D* **35**, 395–424.

Villalba, R.: 1990, 'Climatic Fluctuations in Northern Patagonia in the Last 1000 Years as Inferred from Tree-Ring Records', *Quatern. Res.* **34**, 346–360.

Villalba, R.: 1994, 'Tree-Ring and Glacial Evidence for the Medieval Warm Epoch and the Little Ice Age in Southern South America', *Clim. Change* **26**, 183–197.

Villalba, R.: 2000, 'Dendroclimatology: A Southern Hemisphere Perspective', in Smolka, P. and Volkheimer, W. (eds.), *Paleo- and Neoclimates of the Southern Hemisphere: The State of the Arts*, Springer, Germany, pp. 105–143.

Villalba, R., Boninsegna, J. A., and Cobos. D. R.: 1989, 'A Tree-Ring Reconstruction of Summer Temperature between AD 1500 and 1974 in Western Argentina', *Third International Conference on Southern Hemisphere Meteorology and Oceanography*, Buenos Aires, Argentina, American Meteorological Society, pp. 196–197.

Villalba, R., Boninsegna, J. A., Veblen, T. T., Schmelter, A., and Rubulis, S.: 1997, 'Recent Trends in Tree-Ring Records from High Elevation Sites in the Andes of Northern Patagonia, *Clim. Change* **36**, 425–454.

Villalba, R., D'Arrigo, R. D., Boninsegna, J. A., Lara, A., and Delgado, S.: 'Decade- to Century-Scale Climatic Variability in the South American Sector of the Southern Oceans: Evidence from Tree-Ring Records during the Past Four Centuries', *J. Climate*, submitted.

Villalba, R., D'Arrigo, R. D., Cook, E. R., Wiles, G., and Jacoby, G. C.: 2001, 'Decadal-Scale Climatic Variability along the Extratropical Western Coast of the Americas: Evidences from Tree-Ring Records', in Markgraf, V. (ed.), *Inter-Hemispheric Climate Linkages*, Academic Press, San Diego, Califormia, U.S.A., pp. 155–172.

Von Storch, H.: 1995, 'Spatial Patterns: EOFs and CCA', in von Storch, H. and Navarra, A. (eds.), *Analysis of Climate Variability, Applications of Statistical Techniques*, Springer, Berlin, pp. 259–279.

Vose, R. S., Schmoyer, R. L., Steurer, P. M., Peterson T. C., Heim, R., Karl, T. R., and Eischeid, J. K.: 1992, *The Global Historical Climatology Network: Long-Term Monthly Temperature, Precipitation, Sea Level Pressure, and Station Pressure Data*, ORNL/CDIAC-53, Environmental Science Division, Pub. No. 3912.

WMO: 1998, 'The Global Climate System Review, December 1993–May 1996', Nicholls, J. M. (ed.), *World Climate Data and Monitoring Programme*, WMO No. 856, 95 pp.

Wolodarsky-Franke, A., Lara, A., Aravena, J. C., and Cuq, E.: 2000, 'Dendroclimatology of *Nothofagus pumilio* Treeline Forests in the Aysén Region, Chile (43° to 48° S)', *International Conference on Dendrochronology for the Third Millenium*, Abstracts Vol., Mendoza, Argentina, 249 pp.